Received: 18 June 2022 | Revised: 29 September 2022 | Accepted: 7 October 2022

DOI: 10.1002/glia.24284

GLIA

WILEY

RESEARCH ARTICLE

A subset of OPCs do not express Olig2 during development which can be increased in the adult by brain injuries and complex motor learning

Li-Pao Fang[1] | Qing Liu[1] | Erika Meyer[1,2] | Anna Welle[3] | Wenhui Huang[1] | Anja Scheller[1] | Frank Kirchhoff[1,4] | Xianshu Bai[1]

[1]Molecular Physiology, Center for Integrative Physiology and Molecular Medicine, University of Saarland, Homburg, Germany

[2]Laboratory of Brain Ischemia and Neuroprotection, Department of Pharmacology and Therapeutics, State University of Maringá, Maringá, Brazil

[3]Department of Genetics and EpiGenetics, University of Saarland, Saarbrücken, Germany

[4]Experimental Research Center for Normal and Pathological Aging, University of Medicine and Pharmacy of Craiova, Craiova

Correspondence
Frank Kirchhoff and Xianshu Bai, Molecular Physiology, Center for Integrative Physiology and Molecular Medicine, Building 48, University of Saarland, 66421 Homburg, Germany.
Email: frank.kirchhoff@uks.eu and xianshu.bai@uks.eu

Funding information
Deutsche Forschungsgemeinschaft, Grant/Award Numbers: FOR 2289, HU2614/1-1(ProjectID, 462650276), SPP1757; Unitatea Executiva pentru Finantarea Invatamantului Superior, a Cercetarii, Dezvoltarii si Inovarii, Grant/Award Number: PCE 227; Universität des Saarlandes, Grant/Award Numbers: HOMFORExzellenz2018, Young Investigator Grant

Abstract

Oligodendrocyte precursor cells (OPCs) are uniformly distributed in the mammalian brain; however, their function is rather heterogeneous in respect to their origin, location, receptor/channel expression and age. The basic helix–loop–helix transcription factor Olig2 is expressed in all OPCs as a pivotal determinant of their differentiation. Here, we identified a subset (2%–26%) of OPCs lacking Olig2 in various brain regions including cortex, corpus callosum, CA1 and dentate gyrus. These Olig2 negative (Olig2^{neg}) OPCs were enriched in the juvenile brain and decreased subsequently with age, being rarely detectable in the adult brain. However, the loss of this population was not due to apoptosis or microglia-dependent phagocytosis. Unlike Olig2^{pos} OPCs, these subset cells were rarely labeled for the mitotic marker Ki67. And, accordingly, BrdU was incorporated only by a three-day long-term labeling but not by a 2-hour short pulse, suggesting these cells do not proliferate any more but were derived from proliferating OPCs. The Olig2^{neg} OPCs exhibited a less complex morphology than Olig2^{pos} ones. Olig2^{neg} OPCs preferentially remain in a precursor stage rather than differentiating into highly branched oligodendrocytes. Changing the adjacent brain environment, for example, by acute injuries or by complex motor learning tasks, stimulated the transition of Olig2^{pos} OPCs to Olig2^{neg} cells in the adult. Taken together, our results demonstrate that OPCs transiently suppress Olig2 upon changes of the brain activity.

Abbreviations: BrdU, bromodeoxyuridine; CA1, cornu ammonis 1; Cspg4, chondroitin sulfate proteoglycan 4; CC, corpus callosum; CCA, common carotid artery; ctl, control; DG, dentate gyrus; CTX, cortex; dpi, days post injury; E, embryonic day; FI, fluorescence intensity; GFAP, glial fibrillary acidic protein; GS, glutamine synthetase; hp, hippocampus; KA, kainate; MCAO, middle cerebral artery occlusion; MOp, primary motor cortex; mPFC, medial prefrontal cortex; neg, negative; NG2, neural/glial antigen 2; Olig2, oligodendrocyte transcription factor 2; OPCs, oligodendrocyte precursor cells; p, postnatal day; pos, positive; PDGFRα/Pα, platelet derived growth factor receptor alpha; R26, Rosa26; SEM, standard error of the mean; SO, stratum oriens; SP, stratum pyramidale; SR, stratum radiatum; SWI, stab wound injury; tdT, tdTomato; w, week.

KEYWORDS
acute brain injury, Olig2, oligodendrocyte precursor cells, platelet derived growth factor receptor alpha, proliferation

1 | INTRODUCTION

Oligodendrocyte precursor cells (OPCs) are widely distributed within the central nervous system (CNS), however they are rather a heterogeneous population regarding to their location, origin, age and function (Marisca et al., 2020; Marques et al., 2016; Marques et al., 2018; Spitzer et al., 2019; Viganò et al., 2013). A conserved feature of OPCs is the capability to give rise to oligodendrocytes throughout the life (Trotter et al., 2010). OPC differentiation is tightly regulated by intrinsic and extrinsic factors (Rowitch & Kriegstein, 2010). The basic helix–loop–helix transcription factor Olig2, is one of the pivotal intrinsic determinants for oligodendrocyte specification (Liu et al., 2007; Lu et al., 2000; Lu et al., 2002; Maire et al., 2010; Zhou et al., 2000; Zhou & Anderson, 2002). In Olig2 null mice, OPC formation fails at embryonic and perinatal stages (Ligon et al., 2006; Mei et al., 2013), while overexpression of Olig2 triggers OPC differentiation and precocious myelination (Maire et al., 2010; Wegener et al., 2015). Although Olig2 is widely expressed throughout the oligodendroglial development, its function is rather specific to the cell stage (Mei et al., 2013). For instance, Olig2 expression in OPCs promotes cell differentiation and subsequent myelination, while in newly formed oligodendrocytes Olig2 seems to suppress maturation and myelination. Apart from lineage commitment, Olig2 exerts function in OPC migration. Overexpression of Olig2 accelerates OPC migration, differentiation and subsequently promoted remyelination in the lysolecithin model of multiple sclerosis (Wegener et al., 2015).

Despite of the importance and abundance of Olig2 for the lineage of oligodendrocytes, a proportion of NG2^{pos} cells could not be detected for Olig2 expression in the healthy perinatal (about 1%) and adult cortex (8–30%) (Buffo et al., 2005; Ligon et al., 2006). This NG2^{pos}Olig2^{neg} population was even larger after a stab wound injury (Buffo et al., 2005). These NG2^{pos}Olig2^{neg} cells were defined according to their immunoreactivity to NG2 antibody. Of note, NG2 is also expressed by pericytes under physiological conditions and by a small population of microglia triggered by acute brain injuries (Huang et al., 2014; Huang et al., 2020). In addition, due to the cleavage of the extracellular domain of NG2 protein under pathological conditions, NG2 immunoreactivity per se cannot be referred as NG2 expression. Therefore, it is yet elusive whether or not Olig2^{neg} OPCs exist in the brain. If yes, how does the population develop with age? Are they functionally different to the Olig2^{pos} OPCs?

To address these open questions, we distinguished OPCs from other NG2 expressing cells with immunostaining of platelet derived growth factor receptor α (PDGFRα), a well-established marker of OPCs (Nishiyama et al., 1996). We analyzed different brain regions, for example, cortex, corpus callosum, CA1 and dentate gyrus, at different ages ranging from postnatal day (p) 5–44 weeks. PDGFRα^{pos}Olig2^{neg} population was progressively increased at the first two postnatal weeks, followed by a consistent decline. Derived from Olig2^{pos} cells, Olig2^{neg} cells were never expressing Ki67 and exhibited a less complex morphology. Complex motor learning or acute brain injuries, which are known to stimulate brain activity change, triggered increased the population of Olig2^{neg} OPCs in the adult hippocampus and cortex, respectively. In summary, our study demonstrates that OPCs suppress Olig2 expression upon the change of brain activity.

2 | RESULTS

2.1 | A subset of OPCs does not express Olig2

To investigate whether Olig2-non-expressing OPCs exist or not, we performed immunostaining of PDGFRα (Pα) and Olig2 in coronal section of healthy mouse brain (Figure 1a). At postnatal day (p) 14, we observed a small population of Pα^{pos} cells expressing low level or no Olig2 in various brain regions, including primary motor cortex (MOp, Figure 1b–d), corpus callosum (CC, Figure 1e), CA1 (Figure 1f) and in the dentate gyrus region (DG, Figure 1g). To further characterize these cell subtypes, we classified Pα^{pos} cells into Olig2^{pos} cells with high immunoreactivity (fluorescence intensity [FI] > 10^3, 96.52%) and Olig2^{neg} cells with no Olig2 expression (FI < 10^3, 3.48%) (Supplementary Figure 1 A, B). To minimize misinterpretations attributable to potential masking of antigenic sites of Olig2 by formalin fixation, we compared the density of Pα^{pos}Olig2^{neg} cells by performing immunostaining with antigen retrieval. Employing three different methods, including 10 min incubation in 1% SDS solution, heat treatment in Tris-EDTA buffer (pH 9.0) or citrate buffer (pH 6.0) at 95°C for 30 min, we observed comparable amounts of Pα^{pos}Olig2^{neg} cells in all brain regions (Supplementary Figure 1 C–F). These results indicate that indeed a subset of OPCs do not express Olig2 in several brain regions.

To confirm these Pα^{pos}Olig2^{neg} cells are OPCs, we further performed immunostainings by combining Pα and Olig2 with various cell type specific markers at p14, when the population peaks. All Pα^{pos}Olig2^{neg} cells were immunopositive for NG2 with bona fide OPC morphology (Figure 2a, Supplementary Figure 2 A). However, the majority (about 98%) of Pα^{pos}Olig2^{neg} cells were also negative for Sox10 (transcription factor, another lineage marker of oligodendrocytes) (Figure 2b, Supplementary Figure 2 B). In addition, these cells never expressed markers of mature oligodendrocytes (e.g., APC CC1, Figure 2c, Supplementary Figure 2 C), astrocytes (GFAP, Figure 2d, Supplementary Figure 2 D; GS, Supplementary Figure 2 E), neurons (NeuN, Figure 2e, Supplementary Figure 2 G), microglia (Iba1, Figure 2f, Supplementary Figure 2 F), or precursors (DCX, Figure 2g; Sox2, Figure 2h; Supplementary Figure 2 H). Therefore, our results suggest that Pα^{pos}Olig2^{neg} cells are OPCs/NG2 glia.

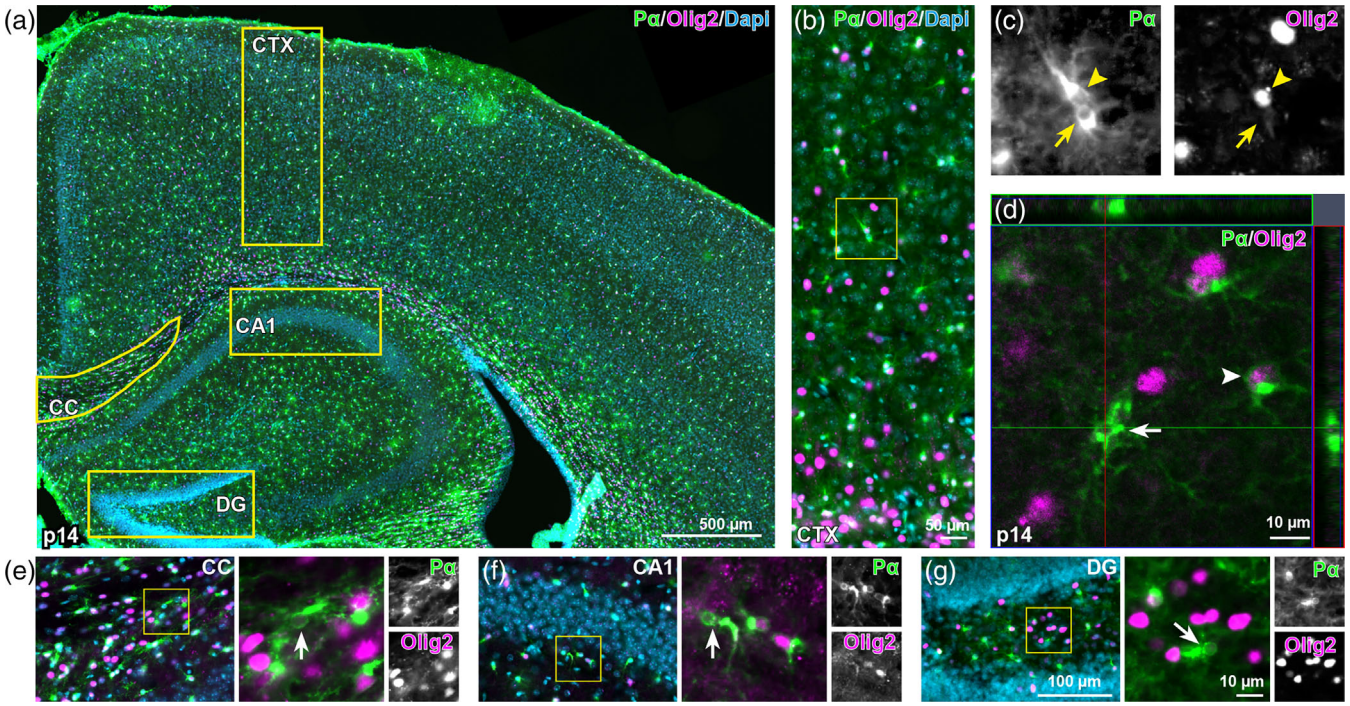

FIGURE 1 A subset of PDGFRα-positive cells do not express Olig2. (a) Overview of PDGFRα (Pα, green) and Olig2 (magenta) immunostaining of coronal brain slices from p14 mice. (b and e–g) Representative images of cortex (CTX), corpus callosum (CC), CA1, and dentate gyrus (DG) stained with Pα and Olig2. (c) Magnified views of $P\alpha^{pos}Olig2^{neg}$ cells from b (boxed area). (d) Confocal images showing $P\alpha^{pos}$ cells without Olig2 expression in cortex. Arrowheads: $Olig2^{pos}$ OPCs, arrows: $Olig2^{neg}$ OPCs.

To further substantiate the lack of Olig2 in a subset of OPCs, we took advantage of NG2-CreER^{T2} x R26-lsl-tdTomato mice, in which OPCs, their descendent oligodendrocytes as well as pericytes express tdTomato (tdT) after tamoxifen induced recombination. Tamoxifen was administered at p7 and 8 (Figure 2i), inducing tdT expression in about 80% of OPCs at p14 (Fang et al., 2022). Again, we observed a small population (about 3%) of $P\alpha^{pos}tdT^{pos}$ cells expressing no Olig2 (Figure 2j,k), confirming that a subset of OPCs do not express Olig2.

2.2 | $Olig2^{neg}$ OPCs are enriched in the juvenile brain

To elucidate whether this cell population exists temporarily or over all ages under physiological conditions, we further analyzed the mice at p5, p9, p14/2 week, 4, 9, 11, 22, and 44 week of age. In MOp, we observed about 1.3 ± 0.2 $Olig2^{neg}$ cells/1×10^{-3} mm^3 at p5 (Figure 3a,g), that is, about 2% of all OPCs (Figure 3h). Progressively, this $P\alpha^{pos}Olig2^{neg}$ cell population increased reaching 3.1 ± 0.8 cells/1×10^{-3} mm^3 (accounting for 7% of all OPCs) at p14 (Figure 3g,h). The same increase was observed in other brain regions (Figure 3g, Supplementary Figure 1 G–J) where $P\alpha^{pos}Olig2^{neg}$ cells were covering 9%, 11%, 13%, and 26% of all OPCs in CC, mPFC, DG, and CA1, respectively (Figure 3h). After p14, the density of $P\alpha^{pos}Olig2^{neg}$ cells continuously decreased. It became rarely detectable in the adult cortex (MOp and mPFC), but it still remained at a rather high level in CC (Figure 3d–f,g,h). Please note, the proportion of $P\alpha^{pos}Olig2^{neg}$ cells among all $P\alpha^{pos}$ cells increased till the fourth postnatal week (Figure 3h), likely due to the reduced pool of $P\alpha^{pos}Olig2^{pos}$ cells during development as observed by us and others (Figure 3i) (Kessaris et al., 2006). Overall, our results indicate that $Olig2^{neg}$ OPCs are present in the brain throughout life, with higher population during the development.

2.3 | $Olig2^{neg}$ OPCs exhibit low proliferative activity

To understand whether the dynamic of the population size was attributed to cell proliferation, cell death or to a transient regulation of Olig2 gene expression, we firstly analyzed apoptosis and phagocytosis of these cells by performing immunostaining of cleaved caspase 3 (CC-3, a well-established marker for apoptosis) (Figure 4a) and CD68 (phagocytic marker, Figure 4b) at p14. Notably, $Olig2^{neg}$ OPCs were neither positive for CC-3 nor for CD68 (Figure 4a,b, Supplementary Figure 3), largely excluding apoptotic loss or microglia mediated elimination of $Olig2^{neg}$ OPCs.

Then, we assessed the proliferation by BrdU incorporation. To distinguish the fast and slowly diving cells, BrdU was administered at 2 h prior to the analysis at p14 or for consecutive 3 days from p12 till p14 (Figure 4c). With the short pulse of BrdU administration, none of the $Olig2^{neg}$ OPCs showed BrdU immunoreactivity in contrast to about 7% of $Olig2^{pos}$ OPCs (Figure 4d,e). Nevertheless, a long-term administration of BrdU labeled about 10% of $Olig2^{neg}$ OPCs with

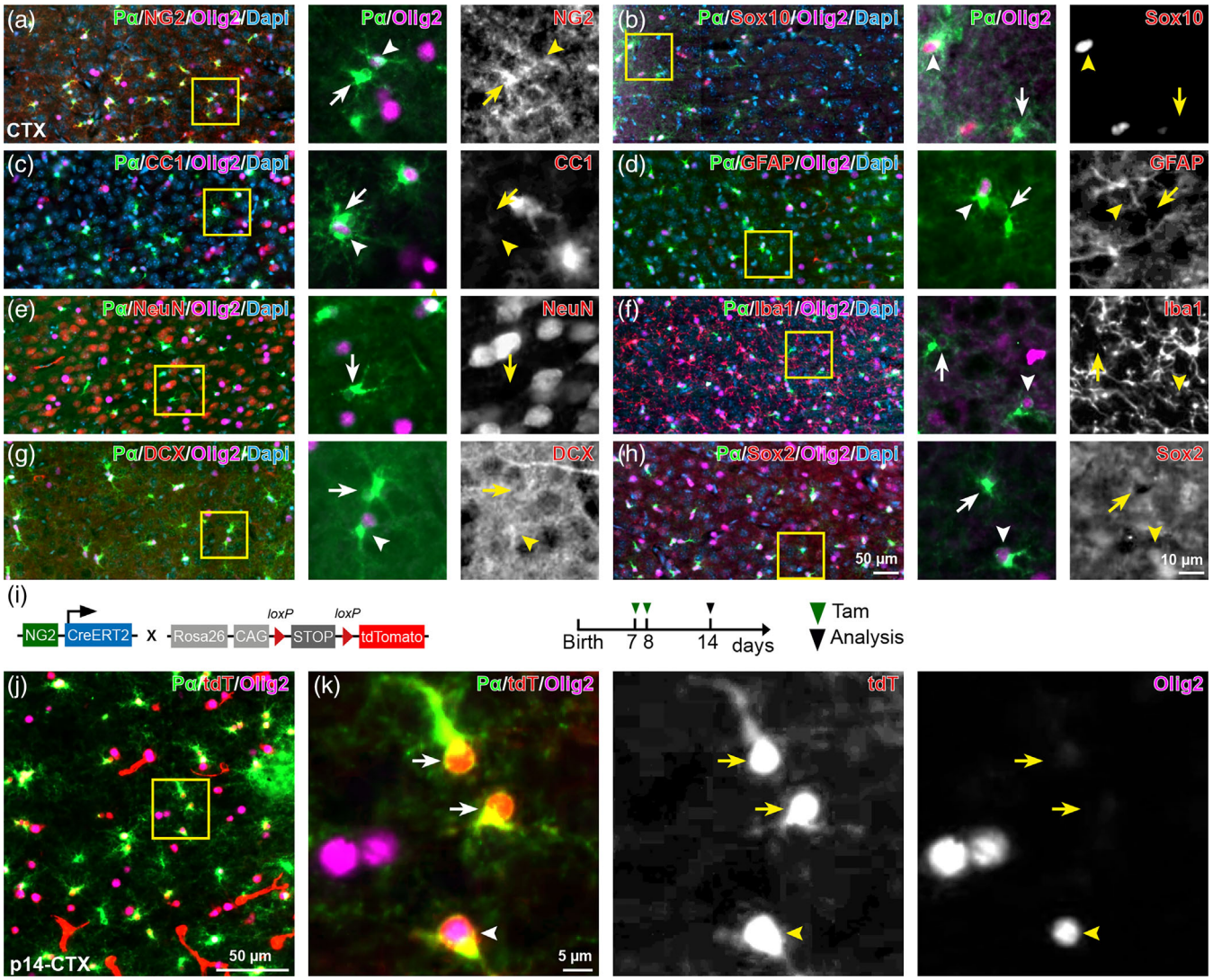

FIGURE 2 PDGFRα^{pos}Olig2^{neg} cells are bona fide OPCs. (a and b) Pα^{pos}Olig2^{neg} cells are immunopositive for NG2 (a), but rarely express Sox10 (b). (c–h) Pα^{pos}Olig2^{neg} cells are not oligodendrocytes (c), astrocytes (d), neuron (e), microglia (f), or neural precursors (g and h). (i) Scheme of transgene construct and experimental schedule. (j) Immunostaining of Pα and Olig2 in the cortex of NG2-CreER^{T2} x R26-tdTomato mice at p14. (k) Magnified views of Pα^{pos}Olig2^{neg} cells expressing tdTomato (tdT) from the area indicated in (j). Arrowheads: Olig2^{pos} OPCs, arrows: Olig2^{neg} OPCs.

BrdU, which was still less than Olig2^{pos} OPCs (29%) (Figure 4d,e), suggesting that Olig2^{neg} OPCs divide very slowly if at all, and are likely derived from Olig2^{pos} OPCs.

To further clarify a potential proliferation capacity of Olig2^{neg} cells, we performed an immunostaining against the mitotic marker Ki67 on these cells at p14 brain (Figure 4f). About 7%–9% of Olig2^{pos} OPCs in the gray matter (MOp, CA1, and DG) and about 28% in the white matter (corpus callosum) (Figure 4g) (arrowheads in Figure 4f) were positive for Ki67, whereas 1.9% of Pα^{pos}Olig2^{neg} cells in MOp (only one cell from a total of 160 cells from 10 mice) and none in CC, CA1 or DG showed immunoreactivity to Ki67 (Figure 4g, Supplementary Figure 4 A) both with or without antigen retrieval (Figure 4g, Supplementary Figure 4 C and D). To substantiate that Olig2^{neg} cells are not proliferative, we applied the same immunohistochemical protocol in the forebrain of embryos at embryonic day (E) 15.5, when the cells are more actively dividing. At E15.5, the first and second wave of OPCs are already generated (Kessaris et al., 2006). We still could detect about 7% of OPCs being Olig2^{neg} (Figure 4h), suggesting Olig2^{neg} is not limited to the third wave of OPCs generated at perinatal days. While the majority of Olig2^{pos} OPCs expressed Ki67, none of the Olig2^{neg} cells expressed Ki67, thereby strongly suggesting a very low-proliferative property of Olig2^{neg} OPCs.

Taken together, our data suggest that Olig2^{neg} cells persist in the adult brain as a distinct subpopulation of oligodendrocyte lineage cells derived from Olig2^{pos} OPCs.

2.4 | Olig2^{neg} cells exhibit a simplified morphology

Since Olig2 is critical for OPC differentiation and subsequent myelination, we asked whether these Olig2^{neg} cells still could generate oligodendrocytes. OPCs increase branching of processes as they

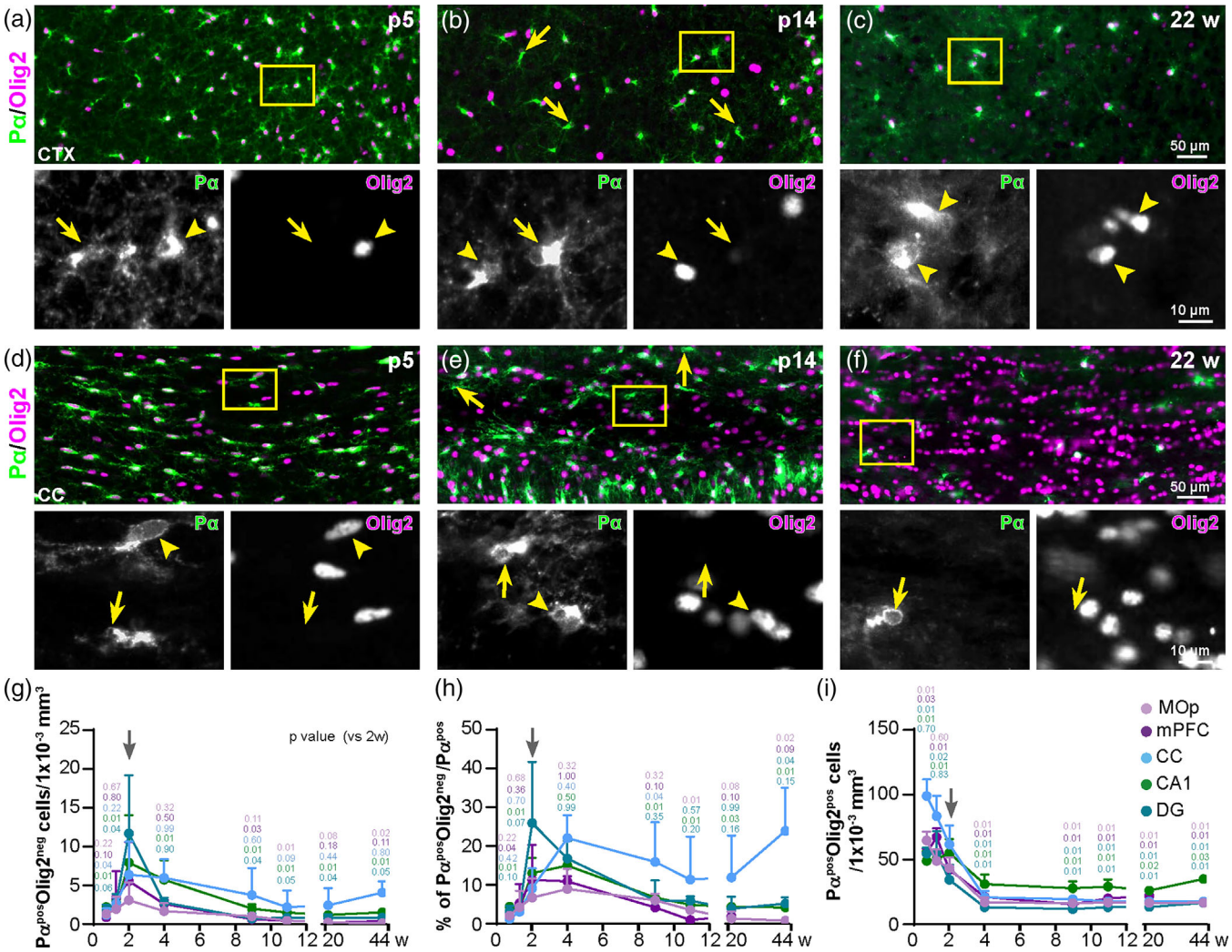

FIGURE 3 Olig2^{neg} OPCs are enriched in the juvenile brain. (a–c) Immunostaining of Pα and Olig2 in the cortex of mice at the age of p5 (a), p14 (b), and 22 weeks (c). (d–f) Immunostaining of Pα and Olig2 in the corpus callosum of mice at the age of p5 (d), p14 (e), and 22 week (f). (g–i) Quantification of density and proportion of Pα^{pos}Olig2^{neg} (g, i) and Pα^{pos}Olig2^{pos} cells (h) reveals maximal population of Pα^{pos}Olig2^{neg} cells in the juvenile brain (primary motor cortex, MOp; medial prefrontal cortex, mPFC; Corpus callosum, CC, CA1, and DG). (p5: $N = 4$ mice (all regions); p9: $N = 4$ mice (all regions); p14: $N = 9$ mice (MOp, CC, CA1, mPFC) and $N = 7$ mice (DG); 4 weeks: $N = 6$ mice (MOp), $N = 4$ mice (CC and mPFC), $N = 5$ mice (CA1), $N = 3$ mice (DG); 9 weeks: $N = 4$ mice (MOp, CC, CA1, DG), $N = 6$ mice (mPFC); 11 weeks: $N = 5$ mice (MOP and CA1), $N = 2$ mice (CC and mPFC), $N = 3$ mice (DG); 22 week: $N = 2$ mice (MOp, CC and CA1), $N = 3$ mice (DG and mPFC); 44 weeks: $N = 3$ (MOp, CC, CA1 and DG), $N = 0$ (mPFC). (within the same brain region, ordinary one-way ANOVA was used for statistical analysis between different time points. Similarly, different brain regions were compared using ordinary one-way ANOVA.) Arrowheads: Olig2^{pos} OPCs, arrows: Olig2^{neg} OPCs.

differentiate into oligodendrocytes (Pfeiffer et al., 1993). Therefore, we compared the morphology of these cells from the p14 cortex using a Sholl analysis based on Pα immunostaining (Figure 5a). We found that Olig2^{neg} OPCs displayed less process branches and shorter total filament length compared to the Olig2^{pos} cells (Figure 5b–d). These data indicate that Olig2^{neg} cells might remain in a precursor stage rather than differentiating into oligodendrocytes.

Studies have suggested that perivascular OPCs exhibit simpler morphologies in comparison to parenchymal ones (Kishida et al., 2019). To understand whether these Olig2^{neg} cells are perivascular OPCs, we labeled endothelial cells of the brain vasculature by PECAM-1/CD31 immunostaining in the p14 brain (Figure 6a, Supplementary Figure 4 B). About 40% of Olig2^{neg} OPCs in CC and 30% in CA1 were located at blood vessels (Figure 6b). However, we also observed a rather low percentage of total Olig2^{pos} OPCs situated perivascular (18.5 ± 8.2% in CC; 16.7 ± 2.7% in CA1). In addition, in cortex and DG, the percentages of these two subtypes at blood vessels were similar (27.7 ± 8.4% [Olig2^{neg}] vs. 25.9 ± 7.0% [Olig2^{pos}] in MOp; 21.3 ± 2.1% [Olig2^{neg}] vs. 15.9 ± 2.8% [Olig2^{pos}] in DG) (Figure 6b). Hence, our results indicate that Olig2^{neg} cells are not necessarily perivascular OPCs, and vice versa. Interestingly, at E15.5 forebrain (about 7% of OPCs were Olig2^{neg}), almost 80% of Olig2^{neg} cells were situated perivascular (Figure 6c–e). This number was 2–3 folds higher than those observed in the adult brain (Figure 6b).

These results indicate that OPCs can down regulate Olig2 and stay in their precursor phase during brain development.

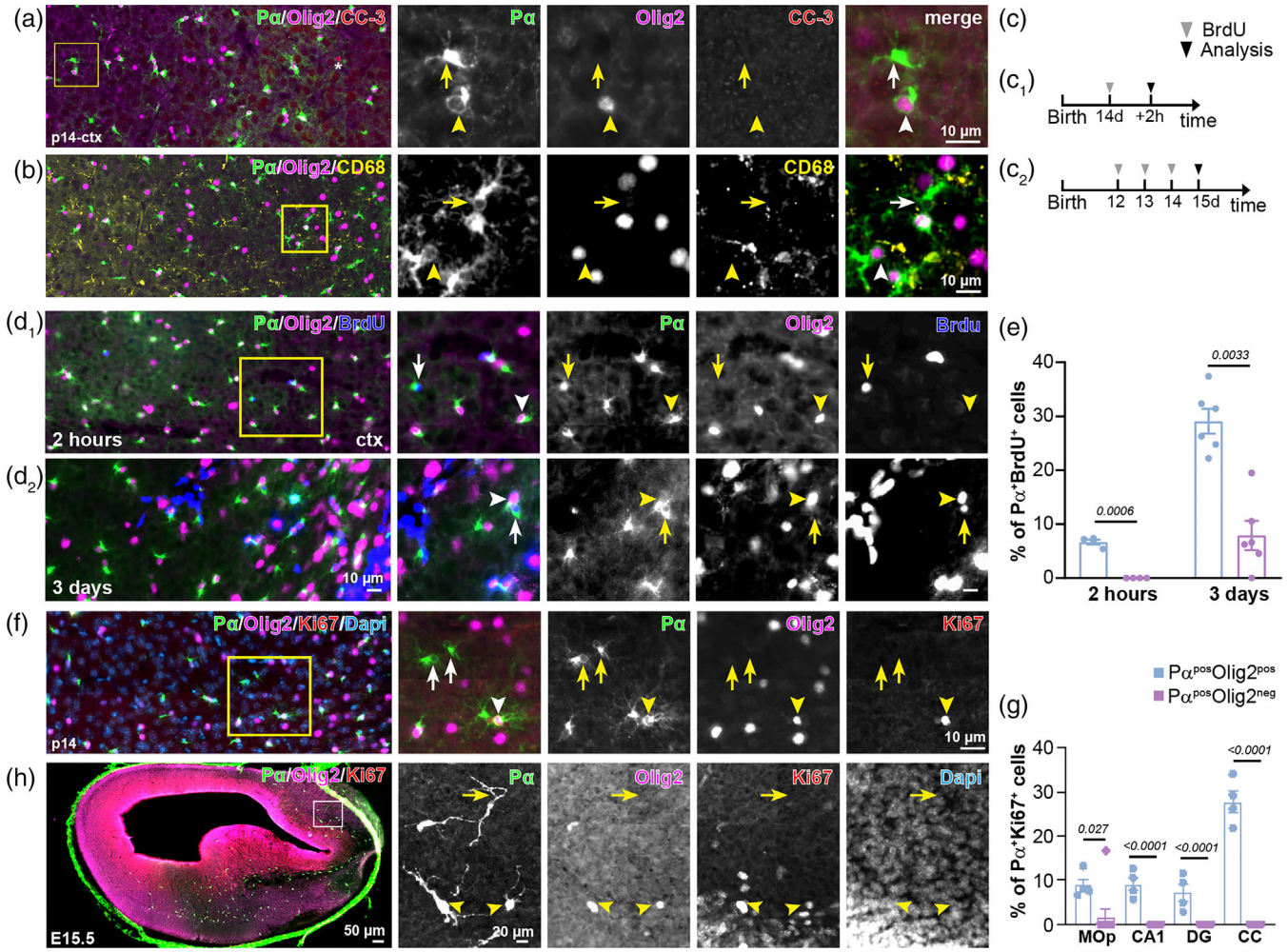

FIGURE 4 Olig2^{neg} cells proliferate less than Olig2^{pos} OPCs. (a) Pα^{pos}Olig2^{neg} cells lacked immunolabeling by apoptotic markers. (b) Pα^{pos}Olig2^{neg} cells are not phagocytosed by microglia. Arrowheads: Olig2^{pos} OPCs, arrows: Olig2^{neg} OPCs. (c) Experimental schedule for BrdU assay (c_1 and c_2) in d_1 and d_2, respectively. (d) Immunostaining of Pα and Olig2 in the cortex of p14 mice after 2 h (c_1, d_1) or 3 days (c_2, d_2) of BrdU administration. (e) Quantification of proliferating Olig2^{pos} and Olig2^{neg} OPCs by BrdU labeling ($N = 4$ mice (2 h), $N = 6$ mice (3 days); two tailed paired t-test). (f and g) Unlike Olig2^{pos} OPCs, Olig2^{neg} OPCs rarely expressed the proliferation marker Ki67 (primary motor cortex, MOp; CA1; dentate gyrus, DG; corpus callosum, CC). ($N = 10$ mice for all brain regions; two-tailed paired t-tests for each brain region). (h) Pα^{pos}Olig2^{neg} cells did not exhibit Ki67 immunoreactivity in the forebrain at embryonic day 15.5. Arrowheads: Olig2^{pos} OPCs, arrows: Olig2^{neg} OPCs.

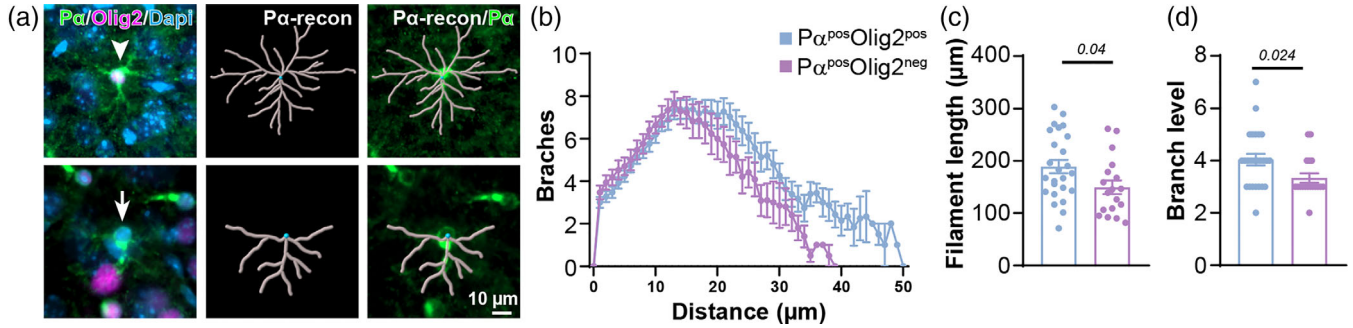

FIGURE 5 Pα^{pos}Olig2^{neg} cells are morphologically less complex than Olig2^{pos} OPCs. (a) Morphological analysis of Olig2^{pos} and Olig2^{neg} OPCs based on Pα immunostaining using Imaris software. (b–d) Sholl analysis showed shorter filament length (b and c) and less branches (b and d) of Olig2^{neg} OPCs. (b: Olig2^{pos} $n = 26$ cells from 4 mice, Olig2^{neg} $n = 23$ cells from 4 mice; c and d: Olig2^{pos} $n = 25$ cells from 4 mice, Olig2^{neg} $n = 23$ cells from 4 mice; two-tailed unpaired t-test)

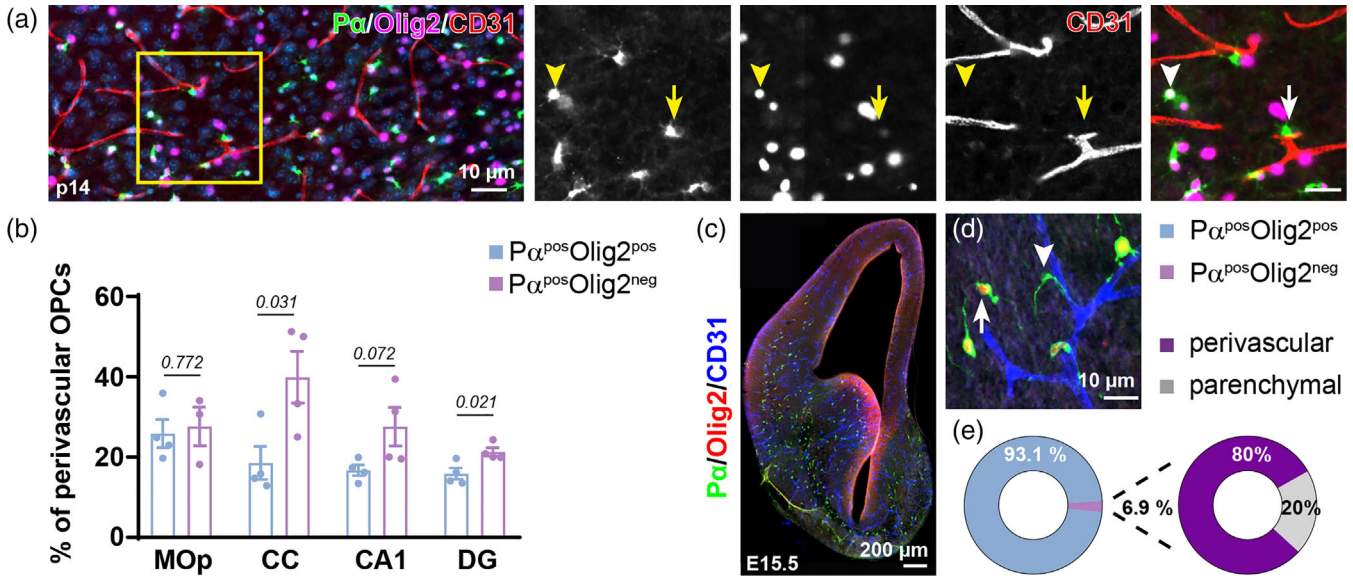

FIGURE 6 In dentate gyrus and corpus callosum Pα^{pos}Olig2^{neg} cells are preferentially located along the blood vessels in comparison to Olig2^{pos} OPCs. (a) Immunostaining of Pα, Olig2, and CD31 at the p14 cortex showed OPCs with or without Olig2 expression adjacent to the blood vessels. (b) Percentage of perivascular OPCs with or without Olig2 from total Pα^{pos}Olig2^{pos} or Pα^{pos}Olig2^{neg} cells in p14 brain, respectively. (MOp: $N = 4$ (Olig2^{pos}) versus 3 (Olig2^{neg}) mice; CC: $N = 4$ mice; CA1: $N = 4$ mice, DG: $N = 4$ mice; two-tailed unpaired t-test). (c and d) Immunostaining of Pα, Olig2, and CD31 in the E15.5 forebrain. (e) Population of Olig2^{neg} OPCs among all OPCs and the percentage of perivascular Olig2^{neg} OPCs from all Olig2^{neg} OPCs at E15.5. ($N = 4$ mice). Arrowheads: Olig2^{pos} OPCs, arrows: Olig2^{neg} OPCs.

2.5 | Increase of Olig2^{neg} OPCs in the adult brain after acute brain injuries

The main establishment of neural networks occurs between birth and p30, which parallels with the emergence of Olig2^{neg} OPCs. OPCs shape neural circuits by participating in synaptic transmission already from p5 and forming connections after differentiation (Bergles et al., 2000; Lin & Bergles, 2004; Orduz et al., 2015). Therefore, we asked whether there could be a causal link between the brain activity status and the formation of Olig2^{neg} OPCs. Therefore, we performed three different types of acute brain injuries in adult mice, when the Olig2^{neg} cell population is rather low. We used stab wound injuries (SWI), kainic acid (KA)-evoked seizures or middle cerebral artery occlusion (MCAO). SWI was induced to 9-week-old mice and analyzed at 3, 7, or 10 days post injury (Figure 7a,b). Already at 3 days post injury (dpi), the density of Pα^{pos}Olig2^{neg} cells in the ipsilateral side, especially at the lesion site (50 μm aside from the lesion), increased 10-fold compared to the contralateral side (34.1 ± 6 vs. 3.5 ± 1 cells/1 × 10^{-2} mm^3, Figure 7c). This number increased further at 7 dpi (75.8 ± 17.5 cells/1 × 10^{-2} mm^3), while returned to the level as 3 dpi at 10 dpi (28.6 ± 1.8 cells/1 × 10^{-2} mm^3) (Figure 7c). KA injection and MCAO also triggered the increase of Pα^{pos}Olig2^{neg} OPC population at the ipsilateral cortex 2 wp KA injection (Figure 7d–f and Supplementary Figure 5 A–C) or in the most affected region (according to the GFAP and Iba1 expression) of the MCAO stroke model (Supplementary Figure 5 D–G). All these data indicate that the formation of Olig2^{neg} cells can be triggered in the adult brain by modifying the brain activity.

To investigate whether these Pα^{pos}Olig2^{neg} cells were derived from pre-existing OPCs or from other precursors, we took advantage of NG2-CreER^{T2} × R26-lsl-GCaMP3 mice where the OPCs can be assessed by evaluating the reporter gene GCaMP3 using GFP antibodies. In addition, compared to the R26-lsl-tdTomato reporter line, GCaMP3 mouse line labels less pericytes after fixation and immunostaining, facilitating a less complex system for OPC visualization among intensive glial and blood cell reaction at the lesion site. Recombination was induced by injection of tamoxifen at the age of 4 weeks. An SWI was performed at the age of 9 weeks (Figure 8a). About 90% OPCs were recombined at the age of 9 weeks (Fang et al., 2022). Analyzed at 3 dpi, all the Pα^{pos}Olig2^{neg} cells in both ipsilateral and contralateral sides were GFP^{pos} (Figure 8b,c), indicating that Pα^{pos}Olig2^{neg} cells were originating from pre-existing GFP^{pos} OPCs, not from other precursor cells. To confirm these hypothesis, we administered BrdU in the drinking water of NG2-CreER^{T2} x R26-lsl-GCaMP3 mice for two consecutive weeks prior to the SWI to label dividing OPCs (Figure 8a). In the contralateral side of 3 dpi cortex, about 47.5% of Olig2^{pos} OPCs were BrdU^{+}, but none of the Olig2^{neg} cells, again excluding a proliferative capacity of Olig2^{neg} cells. However, at the lesion site, 7% of Pα^{pos}GFP^{pos}Olig2^{neg} OPCs had incorporated BrdU (Figure 8b,c). Further immunostaining showed that Olig2^{neg} OPCs did not express Ki67 at 3 dpi (Figure 8c), as observed under physiological conditions, suggesting their origin from pre-existing OPCs after acute brain injuries.

Taken together, our data demonstrate that acute brain injuries can induce the generation of Olig2^{neg} OPCs from Olig2^{pos} OPCs.

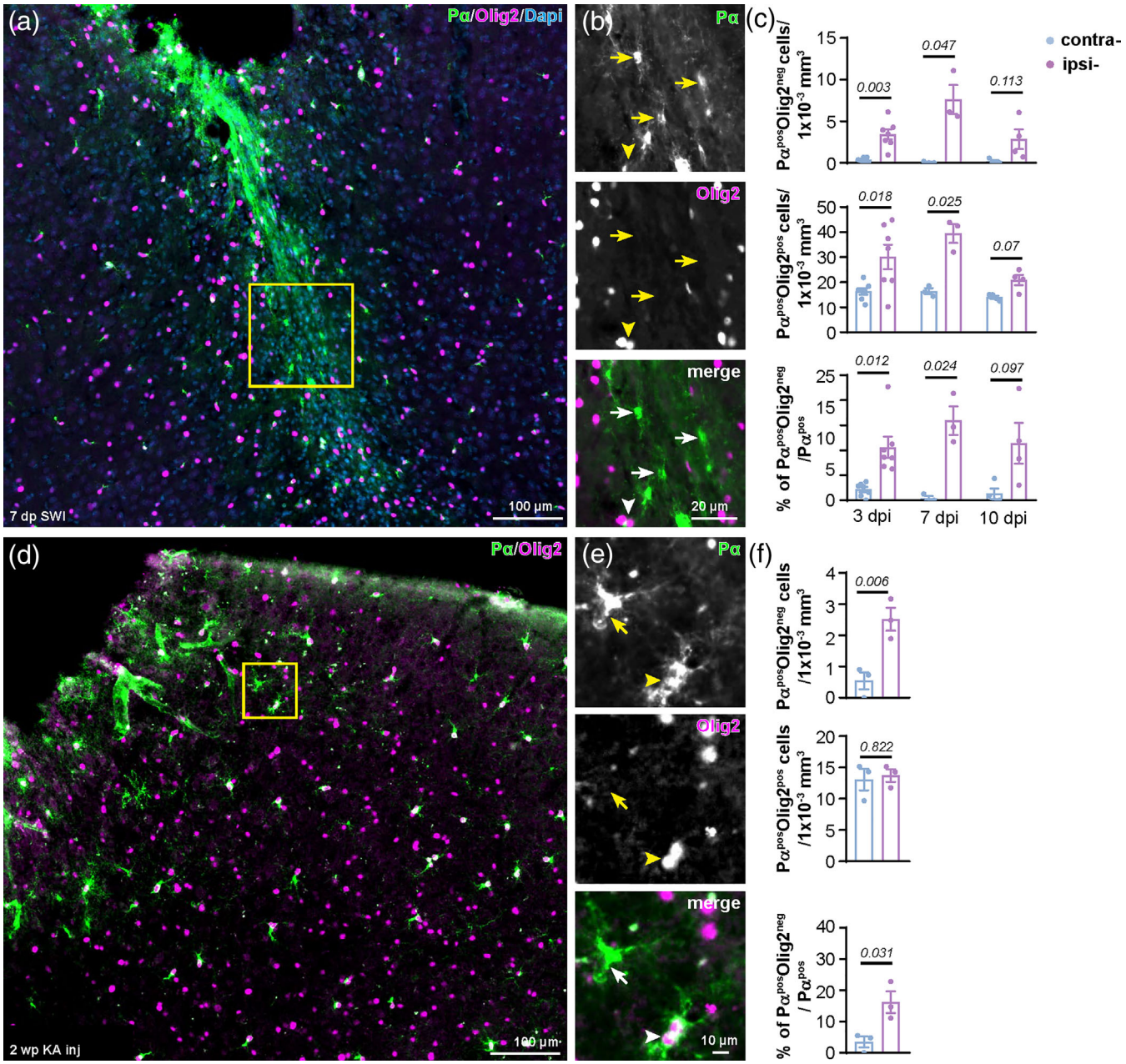

FIGURE 7 Cortical brain injuries trigger the new formation of $P\alpha^{pos}Olig2^{neg}$ OPCs at the lesion site. (a and b) Immunostaining of Pα and Olig2 at the ipsilateral side after 7 days of stab wound injury (SWI) shows numerous $P\alpha^{pos}Olig2^{neg}$ OPCs at the lesion site. (c) Quantification of $Olig2^{neg}$ and $Olig2^{pos}$ OPCS cell density, as well as the proportion of $P\alpha^{pos}Olig2^{neg}$ cells among all OPCs in the contralateral and ipsilateral side at 3, 7, and 10 days post SWI. (3 dpi: $N = 7$, 7 dpi = 3, 10 dpi = 4 mice; two-tailed paired t-test). (d and e) Immunostaining of Pα and Olig2 at the ipsilateral side of kainate injected cortex 2wpi. (f) Cell densities of $Olig2^{neg}$ and $Olig2^{pos}$ OPCs, and the percentage of $Olig2^{neg}$ cells in the contralateral and ipsilateral side at 2 wpi of kainate. ($N = 3$ mice, two-tailed paired t-test). Arrowheads: $Olig2^{pos}$ OPCs, arrows: $Olig2^{neg}$ OPCs.

2.6 | The formation of $Olig2^{neg}$ OPCs is related to the establishment of neural networks

To substantiate that $Olig2^{neg}$ OPCs are required for the plastic formation of functional neural networks, we challenged mice with a 3-week complex running program on the Erasmus Ladder (Van Der Giessen et al., 2008). After 5 days of habituation, mice at 8 or 19 weeks of age had to run the ladder with random cues and obstacles for consecutive 16 days (Figure 9a). To correlate the learning and the appearance of $Olig2^{neg}$ OPCs, immunostaining was performed at three different time points: before learning (right after habituation, day 5), middle of learning (day 13) and end of learning (day 21) (Figure 9a, Supplementary Figure 6 A). Quantification of missteps showed that the mice could run properly only at the last few days of the learning (Supplementary Figure 6 B). Learning a complex running program combines basic motor activity and learning. Therefore, motor cortex and hippocampus

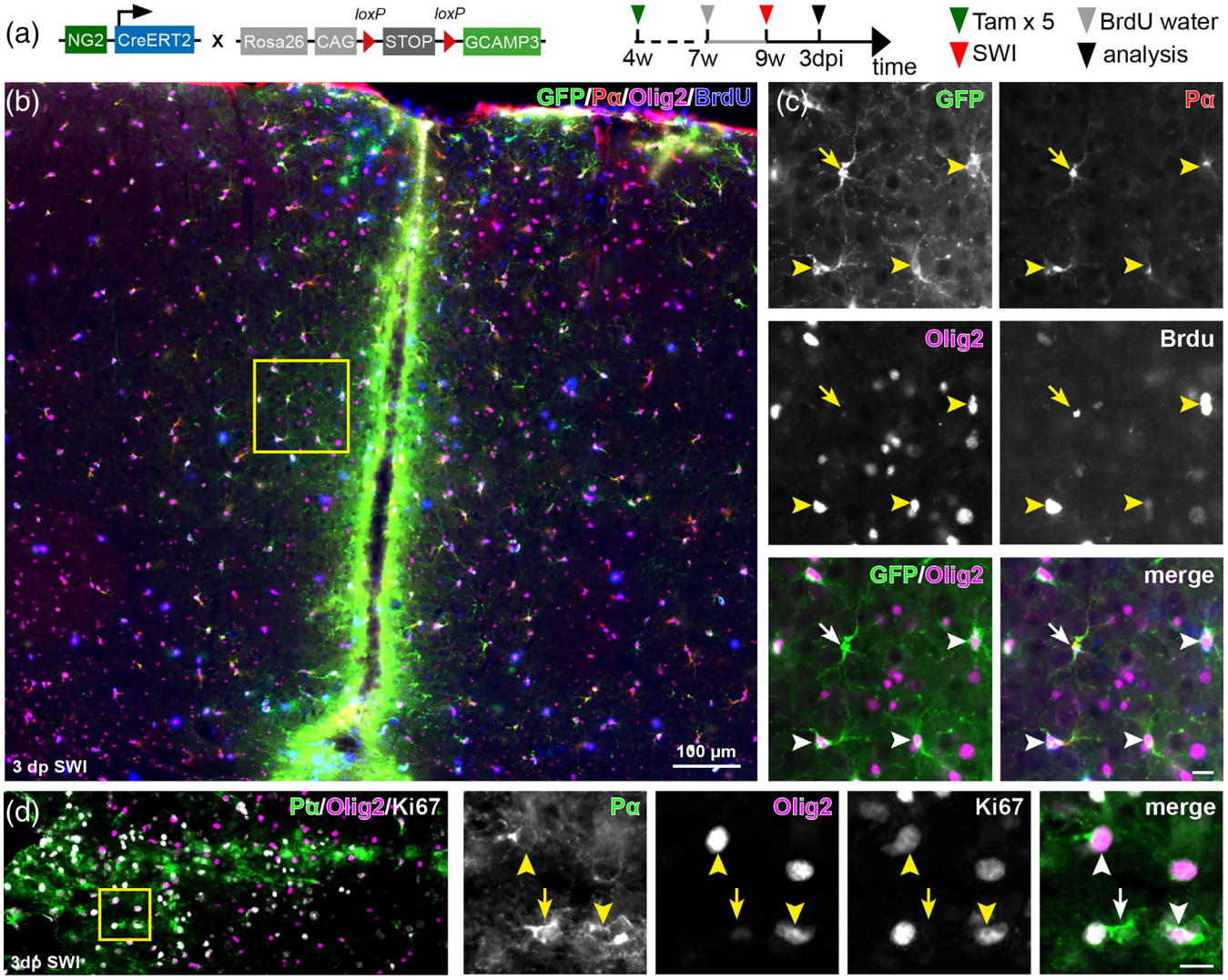

FIGURE 8 OPCs transiently suppress Olig2 after acute brain injury. (a) Scheme of transgene structure and experimental design for b and c. (b) Immunostaining of GFP, Pα, Olig2, and BrdU at the lesion site 3 dpi. (c) Representative images showing that $GFP^{pos}P\alpha^{pos}$ OPCs with (arrowhead) or without Olig2 (arrow) expression incorporated with BrdU. (d) Immunostaining of $P\alpha^{pos}Olig2^{neg}$ OPCs by the mitotic marker Ki67 in the lesion site at 3 days post stab wound injury (dpi SWI). Arrowheads: $Olig2^{pos}$ OPCs, arrows: $Olig2^{neg}$ OPCs.

were primarily analyzed for the $Pa^{pos}Olig2^{neg}$ cell population, both brain regions closely related to motor activity and learning in the forebrain (Burman, 2019; Jacobacci et al., 2020). In the hippocampus, while the density of $Pa^{pos}Olig2^{neg}$ cells increased 2–4 times in both DG and CA1 region compared to control animal after complete learning session (Figure 9a–d), no change was observed before or during the early learning period (Supplementary Figure 6 C–E). In addition, the population of $Olig2^{neg}$ OPCs remained stable in the motor cortex, somatosensory cortex or CC (Supplementary Figure 6 F–J). These results suggest that the formation of $Olig2^{neg}$ OPCs in the hippocampus is likely related to learning induced novel neural networks.

In summary, our results indicate that a subset of OPCs transiently downregulate Olig2 upon micro-environmental changes, contributing further to OPCs heterogeneity.

3 | DISCUSSION

Olig2, a basic helix loop helix transcription factor, is a critical determinant for oligodendrocyte lineage function, specification, and differentiation. However, here, we observed a subset of OPCs that lack Olig2 throughout life in the brain, in gray as well as in white matter regions such as cortex, hippocampus or corpus callosum. Emergence of this population coincided with brain activity changes. Unlike $Olig2^{pos}$ OPCs, $Olig2^{neg}$ cells exhibited very low (if any) self-renewing activity and a simplified morphology in the developing brain, suggesting a putative functional difference between these two subpopulations. Overall, our study demonstrated that upon the change of brain activity, a subset of OPCs transiently shutdown Olig2 expression.

OPCs receive glutamatergic and GABAergic input from neurons and differentiate into oligodendrocytes (Bergles et al., 2000; Gautier

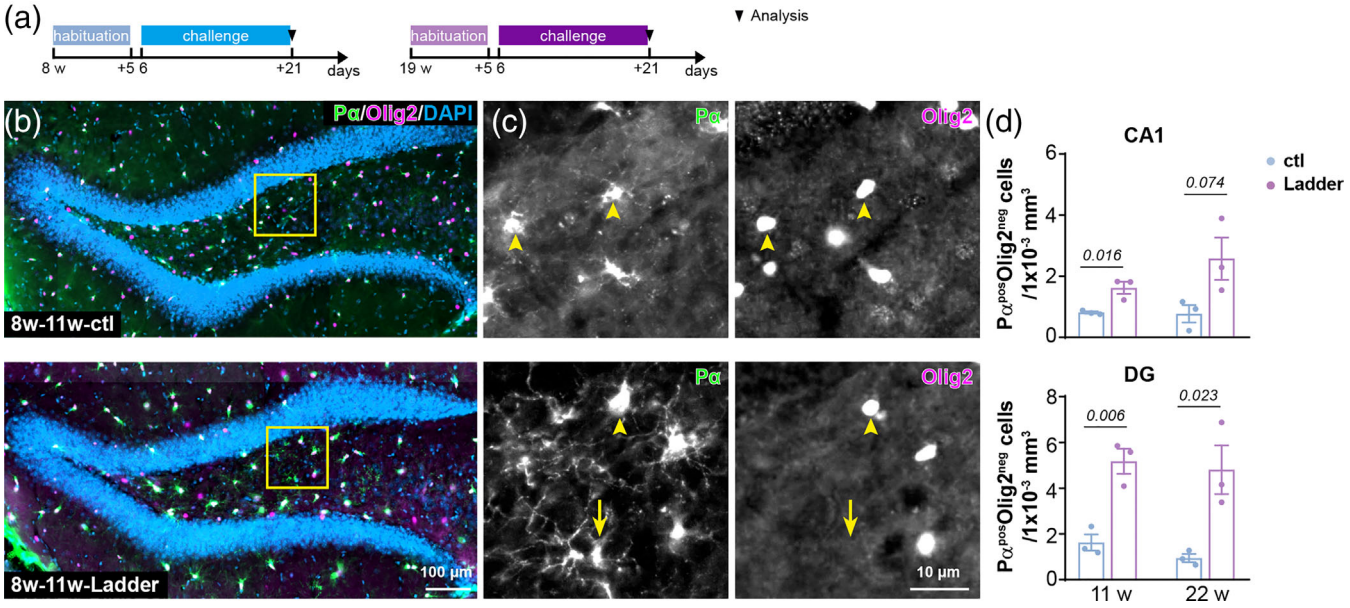

FIGURE 9 Complex motor learning increases the formation of $P\alpha^{pos}Olig2^{neg}$ OPCs in the adult hippocampus. (a) Experimental schedule. (b) Overview of hippocampus immunostained with Pα and Olig2 in the control and trained mice. (c) Magnified views of the area indicated in b show OPCs ($P\alpha^{pos}$) with (arrowhead) or without (arrow) Olig2 expression. (d) Quantification of $P\alpha^{pos}Olig2^{neg}$ cell density in the CA1 and DG region in the control and Erasmus ladder trained mice at 11 or 22 weeks. ($N = 3$ mice, two-tailed unpaired t-test). Arrowheads: $Olig2^{pos}$ OPCs, arrows: $Olig2^{neg}$ OPCs.

et al., 2015; Orduz et al., 2015; Serrano-Regal et al., 2020). Not only, OPCs also shape neural circuits (Fang et al., 2022; Xiao et al., 2022; Zhang et al., 2021). For instance, prior to myelin onset, the large population of OPCs in mouse medial prefrontal cortex release TNF like weak inducer of apoptosis (TWEAK) to optimize interneuron population which is pivotal for proper neural network activity (Fang et al., 2022). In addition, as seen in zebrafish optic tectum, a subtype of OPCs remain precursors throughout life and control axonal remodeling, never differentiating into myelinating oligodendrocytes (Xiao et al., 2022). A recent study has demonstrated that a set of genes, involved in pathways including neuronal differentiation and brain development, are repressed by Olig2 to ensure OPC differentiation into oligodendrocytes (Zhang et al., 2022). Therefore, it is tempting to speculate that OPCs switch off Olig2 expression and remain as precursors or NG2 glia upon the change of brain activity. Indeed, we observed a less complex morphology of $Olig2^{neg}$ cells in comparison to $Olig2^{pos}$ cells, suggesting $Olig2^{neg}$ OPCs yet exhibit less potential to commit the differentiation.

In general, neural plasticity is greater in the developing brain than in the adult, and learning a new skill or brain injuries could boost neural circuit reorganization (Galván, 2010; Su et al., 2016). The appearance of $Olig2^{neg}$ OPCs in the postnatal brain coincided with the development of neuron-OPCs connectivity starting from postnatal day 4–5 and reaching a peak at p10 for cortical interneurons (Orduz et al., 2015). Complex motor learning processes as well as acute brain injuries evoked novel formation of $Olig2^{neg}$ OPCs. Interestingly, BMP4, known to repress Olig2 expression, is essential for synapse plasticity and is upregulated during brain development and after injuries (Bai et al., 2021; Higashi et al., 2018). Therefore, BMP4 might be involved in the downregulation of Olig2 in OPCs during neural circuit establishment and to keep OPCs in precursor stage and innervate into neural circuit. Nevertheless, $Olig2^{neg}$ cells were more frequently observed in white matter areas such as corpus callosum than in the gray matter of cortex or hippocampus. This could be attributable to inherited intrinsic programs (Viganò et al., 2013; Viganò & Dimou, 2015) and/or microenvironmental variations. E.g., the corpus callosum exhibits higher stiffness than gray matter, and such high stiffness hinders OPCs proliferation and differentiation (Segel et al., 2019). However, the $Olig2^{neg}$ OPC population wanes with age, albeit the brain stiffness increases with age (Segel et al., 2019). Hence, molecular mechanisms involved in the generation of $Olig2^{neg}$ OPCs needs to be further studied.

Taking advantage of NG2-CreER^{T2} mice, we found that $Olig2^{neg}$ OPCs were derived from pre-existing OPCs downregulating Olig2 upon acute brain injuries. Interestingly, different to the $Olig2^{pos}$ cells, $Olig2^{neg}$ OPCs were rarely recognized by Ki67 antibody at any brain region. Indeed, Olig2 directly activates cell proliferating pathways to facilitate tumor growth in proneural glioma (Lu et al., 2016). Single cell RNA sequencing database of zebrafish and mouse brain have also suggested a subgroup of $PDGFR\alpha^{pos}$ OPCs that apparently lack expression of Olig2 and the mitotic marker Ki67 (Figure 10a) (Marisca et al., 2020; Marques et al., 2016). By analyzing the published database (https://mouse-oligo-het.cells.ucsc.edu) (Marques et al., 2016), we identified slightly higher numbers of OPCs without Olig2 mRNA (31.6% (database) vs 10–25% (own data), Figure 10d) and also similarly large proportion of these cells not expressing Ki67 (91%

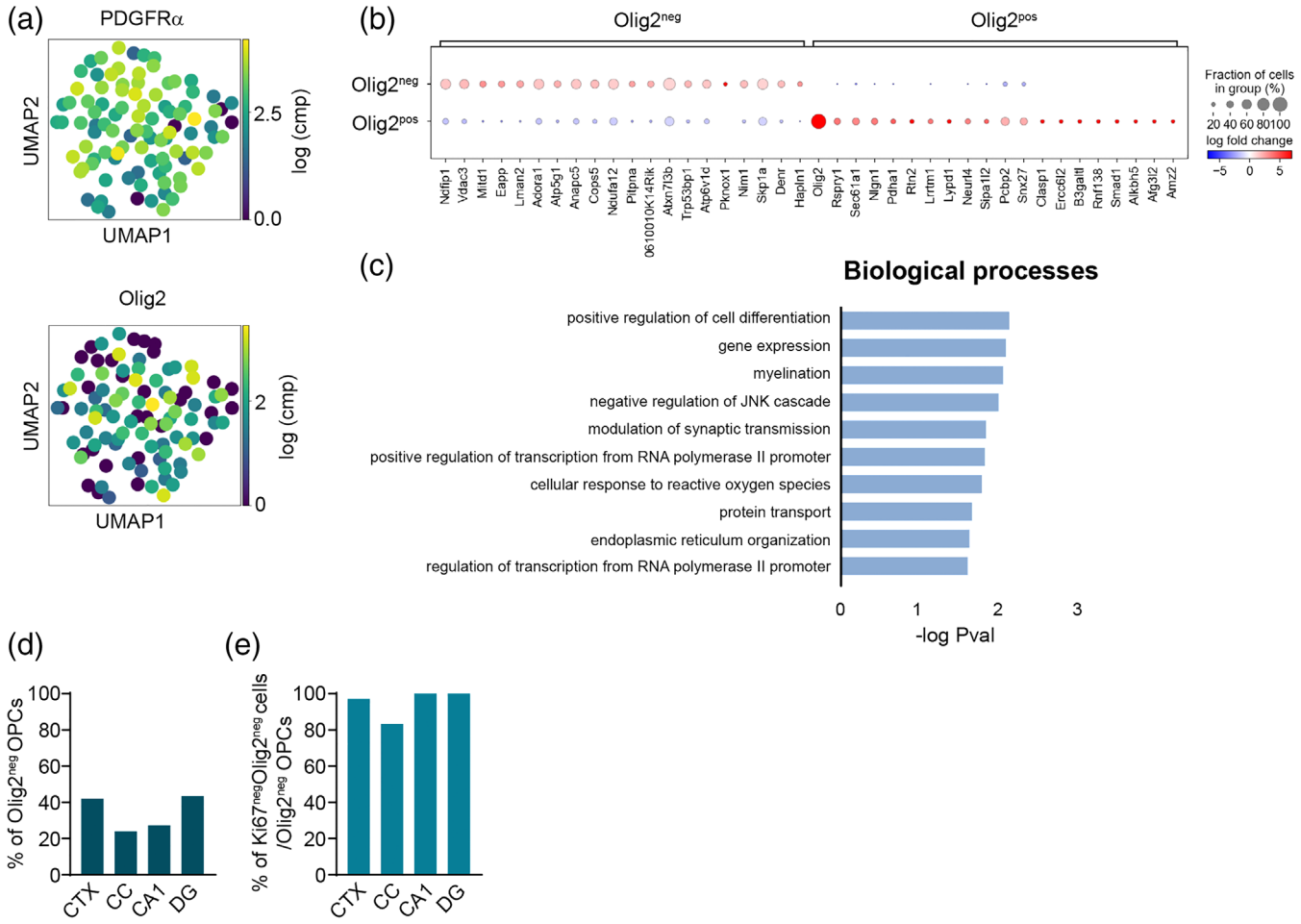

FIGURE 10 Cell differentiation and myelination is suppressed in Olig2^{neg} OPCs. (a) UMAP dimension reduction representation of single OPCs for PDGFRα and Olig2 expression from published database (Marques et al., 2016). (b) Dot plot visualizing differential gene expression between Olig2^{neg} and Olig2^{pos} OPCs. (c) Biological processes enriched for genes that are higher expressed in Olig2^{pos} OPCs. (d and e) Quantification of OPCs expressing no Olig2 (expression level = 0) (d) and Olig2^{neg} OPCs expressing no Ki67 (e) in cortex (CTX), corpus callosum (CC), CA1 and dentate gyrus (DG) from the data source of (Marques et al., 2016).

(database) vs 98–100% (own data), Figure 10e). In addition, in the zebra fish spinal cord, the "cluster #1" OPCs were also found to be negative for Ki67, considered as "quiescent" OPCs since they lacked proliferation and differentiation related markers (Marisca et al., 2020). Instead, these cells were enriched with mRNAs involved in axon guidance and synaptic communication (Marisca et al., 2020). Hence, if Olig2^{neg} OPCs represent similar "quiescent" OPC population in the mouse brain, these cells might be also well integrated into neural circuit. By comparing the genes differently expressed in Olig2^{pos} and Olig2^{neg} OPCs using published single cell transcriptomic data (Marques et al., 2016) (https://mouse-oligo-het.cells.ucsc.edu), we observed 59 genes enriched in Olig2^{neg} OPCs and 400 for Olig2^{pos} cells (Supplementary File S1, top 20 genes for each population are listed in Figure 10b). In Olig2^{neg} cells, for example, adenosine A1 receptor (A1AR, *Adora1*) was enriched compared to Olig2^{pos} cells, suggesting a potential purinergic signaling involved in suppression of Olig2 in OPCs. Shown by gene ontology (GO) analysis, genes positively regulating cell differentiation and myelination, eg. *Olig2*, *Mbp*, *Egr2* were highly enriched in the Olig2^{pos} cells (Figure 10c). Nevertheless, whether Olig2^{neg} OPCs are a functionally and physiologically different group of OPCs needs additional further characterization, for example, by electrophysiology or patch-sequencing. Developmentally, OPCs are generated in three waves: at E12.5 from Nkx2.1^{pos} precursors, at E14.5 from Gsx2^{pos} precursors and from Emx1^{pos} precursors at perinatal days (Kessaris et al., 2006). After birth, the first wave of OPCs, especially in the dorsal cortex, disappear within the first two postnatal weeks, matching to the time points when Olig2^{neg} OPCs start to appear. However, we did not observe Olig2^{neg} OPCs expressing cleaved caspase-3 or being phagocytosed by microglia. In addition, Olig2^{neg} OPCs can also exist in the embryonic brain (detected at E15.5), when yet no OPC death was reported. Nonetheless, we do not exclude other mechanisms eliminating OPCs thereby transiently becoming PDGFRα^{pos}Olig2^{neg} cells, when PDGFRα is yet not fully degraded whereas Olig2 already is. However, the half-life of PDGFRα is 3 h in the absence of ligands and that of Olig2 is in the range of 4–8 h, at least *in vitro* (Coats et al., 1994; Kupp et al., 2016).

Unfortunately, these Olig2^{neg} OPCs are not able to be fate-tracked by live imaging techniques, since Olig2^{neg} OPCs can, so far, only be recognized by the immunostaining.

At the early postnatal brain Olig2 is mainly expressed by oligodendrocyte lineage cells and a subtype of astrocytes (Cai et al., 2007; Wang et al., 2021). Subsequently, astrocytes progressively downregulate Olig2 during their postnatal development, thereby Olig2 becomes restricted to the oligodendrocyte lineage (Lu et al., 2000; Takebayashi et al., 2002; Zhou et al., 2000). However, under pathological conditions, Olig2 expression alters and the expressing population even extends to other cell types, for example, astrocytes (Chen et al., 2008). Olig2 is essential for the astrogliosis after cortical injuries (Chen et al., 2008). Deletion of Olig2 specifically in OPCs induced the differentiation into astrocytes rather than into oligodendrocytes (Zhu et al., 2012). Several studies have indicated that OPCs differentiate into astrocytes upon acute brain injuries (Bai et al., 2021; Dimou et al., 2008; Komitova et al., 2011; Scheller et al., 2017; Tatsumi et al., 2008). Therefore, it is possible that these Olig2^{neg} OPCs switch their fate and give rise to astrocytes. However, fate mapping with NG2-CreER^{T2} mice did not show any reporter positive astrocytes in the physiological brain, also not after the peak of Olig2^{neg} OPCs appearance. Therefore, additional studies are necessary to investigate the function of Olig2^{neg} OPCs. This might provide a novel insight for the understanding of neuron-OPCs communication under physiological and pathological conditions.

4 | MATERIALS AND METHODS

4.1 | Ethics statement

All animal experiments were carried out at the University of Saarland in strict accordance with recommendations of European and German guidelines for the welfare of experimental animals. Animal experiments were approved by Saarland state's "Landesamt für Gesundheit und Verbraucherschutz" in Saarbrücken/Germany (animal license numbers: Perfusion 2020–2025, 36/2016, 03/2021, 08/2021).

4.2 | Animals

All mouse lines were maintained in C57BL/6N background and housed with a 12 hour (h) light/dark cycle at 20°C in the animal facility of the CIPMM. Mice were fed a breeding diet (V1125, Sniff) ad libitum. For the developmental study, C57BL/6N animals were analyzed at the age of postnatal day 5 (P5), P9, 2, 4, 9, 11, 22, and 44 weeks, while embryos were analyzed at E15.5. To follow the fate of OPCs, we took advantage of NG2-CreERT2 knock-in mice carrying CAG-^{fl}STOP^{fl}-tdTomato (TgH[ROSA26-CAG-fl-stop-fl-tdTomato]) or CAG-^{fl}STOP^{fl}-GCaMP3 (TgH[ROSA26-CAG-fl-stop-fl-GCaMP3]) reporter (W. Huang et al., 2014; Madisen et al., 2010; Paukert et al., 2014). Mice were always heterozygous for NG2-CreER^{T2} and homozygous for the floxed reporter loci. Data from both genders were pooled together without bias.

4.3 | Tamoxifen induced recombination

Tamoxifen (Carbolution, Neunkirchen, Germany) was dissolved in Miglyol®812 (Caesar & Lorentz GmbH, Hilden, Germany) to a final concentration of 10 mg/ml and administrated intraperitoneally for two consecutive days at postnatal day 7 and 8 or for five consecutive days at the age of 4 weeks (Fang et al., 2022; Jahn et al., 2018).

4.4 | Erasmus ladder

Complex motor learning was performed using the Erasmus Ladder (Noldus Technology) as previously described with modifications (Saab et al., 2012; Van Der Giessen et al., 2008). Individual test mice were placed in a dark shelter. With a light cue and 3 s delayed air cue, the animal was encouraged to run over the ladder and reach the shelter at the other side. One trial was defined as a single ladder crossing from one shelter to another, and one session was composed of 42 trails. Each mouse performed one session per day. The first 5 days were regarded as training sessions followed by 16 days of challenging sessions. At training sessions, mice were habituated with the ladder and the cues. From the sixth day, during ladder running mice were randomly perturbed by single sounds or obstacles, or combinations of sound and obstacles. Only one or no perturbation was added per trial. The duration time of steps per trial was automatically recorded.

4.5 | Stab wound injury

Stab wound injuries (SWI) were performed on 9–12 weeks old mice as described previously (Bai et al., 2021). Briefly, mice were anesthetized with a mixture of 2% Isoflurane and 49% O_2 and 49% N_2O via inhalation and the skull was thinned with a dental drill laterally 1.5 mm and longitudinally 2 mm from Bregma. A 1 mm deep stab wound was made by the insertion of surgical scalpel into the somatosensory cortex. The skin was sutured and buprenorphine/carprofen was intraperitoneally/subcutaneously given for three consecutive days. Tramadol (0.4 mg/ml) was administered in drinking water for seven consecutive days. Mice were analyzed at 3, 7, and 10 days post injury (dpi).

4.6 | Middle cerebral artery occlusion

MCAO was performed as previously described (W. Huang et al., 2020). Mice were anesthetized with inhalation anesthetics as described above. Breifly, the left common carotid artery (CCA) and the external carotid artery were ligated with silk sutures and an arteriotomy was performed on the CCA. Then a silicon-coated filament (Doccol Corp, CA) was inserted into the CCA and advanced through the internal carotid artery until it reached the origin of the middle cerebral artery. After 15 min of occlusion, reperfusion was obtained by withdrawal of the filament. Lastly, another suture was made around the CCA, to prevent back flow through the arteriotomy.

Mouse body temperature was continuously monitored using a rectal thermometer and an adjustable heat plate. Mice received buprenorphine/carprofen for pain relief and subcutaneous injection of 0.5 ml saline as fluid replacement for three consecutive days. Tramadol (0.4 mg/ml) was administered in drinking water for 7 consecutive days. Mice were analyzed at 3 dpi.

4.7 | Kainate injection

Cortical kainate injections were performed unilaterally as described previously (Bedner et al., 2015). Briefly, 70 nl of 20 mM kainic acid in saline was injected to the right hemisphere of anesthetized mice, at the position of AP:-1.92 mm, ML: 1.5 mm, DV: 1 mm referred to the bregma. Proper analgestic treatment was performed as ment Tramadol (0.4 mg/ml) was administrated in drinking water for 7 consecutive days. Mice were analyzed at 1 and 14 dpi.

4.8 | Immunohistochemistry

Mice were perfused with PBS followed by 4% PFA. After post fixation, coronal vibratome slices in 40 μm thickness were collected. After 1 h incubation with blocking buffer (5% horse serum with 0.5% Triton in PBS), free floating slices were incubated with primary antibodies at 4 °C overnight, followed by secondary antibody incubation. DAPI (25 ng/ml) was used to stain nuclei (A10010010, Biochimica). Primary and secondary antibodies are listed in the Supplementary Tables 1 and 2, respectively.

4.9 | Antigen retrieval treatment

Prior to the blocking step, the following treatments were performed:

SDS treatment: Slices were incubated with 1% SDS buffer (in 1x PBS) for 10 min and washed subsequently with 1x PBS for 5 min by three times (Q. Liu et al., 2022).

Heat treatment in Tris-EDTA buffer (pH = 9.0) or citrate buffer (pH = 6.0): Slices were attached to the slides in a proper sized slide container filled with 1 X Tris EDTA buffer (10 mM Tris base and 1 mM EDTA) or citrate buffer (10 mM citric acid and 0.05% Tween 20). The container was placed in water bath at temperature above 95°C for 30 min. After cooling to room temperature for 20 min, slices were blocked for primary antibody incubation. These two treatments were suggested by the website (Patel et al., 2020; Wimmer et al., 2019).

4.10 | Bromodeoxyuridine assay

For adult animals, 1 mg/ml BrdU was administered in the drinking water for 2 weeks before the surgery. For short pulse labeling, 10 mg/ml BrdU saline solution was intraperitoneally injected to the mice 2 h prior to the analysis. For BrdU immunostaining, after washing off the secondary antibody, slices were fixed with 2% PFA at room temperature (RT) for 15 min, followed by washing with 1x PBS twice and once by distilled water. Slices were then incubated with 2 M HCl at 37°C for 45 min. After three times washing, slices were incubated with primary BrdU antibody and secondary antibodies as described above.

4.11 | Microscopic analysis and quantification

Two brain slices per mouse and at least three animals per group were analyzed. Images were obtained with an automated slide-scanning epifluorescence microscopy system (Zeiss AxioScan Z1, for overviews) or a confocal laser-scanning microscope (Zeiss LSM-710, for high-resolution and image stacks).

For quantification of fluorescence intensity of Olig2 and PDGFRα, slices scanned with the AxioScan Z1 were analyzed using ZEN 3.1 (blue edition, Zeiss) software. When the Olig2 fluorescence intensity was comparable to background value (between 1×10^2 and 1×10^3), it was considered as Olig2^{neg} OPC (Supplementary Figure 1 A). To account for variability in the staining from different animal, all values of Olig2 and PDGFRα were directly compared with values of the background in the same brain section.

4.12 | Single cell RNA sequencing analysis

Source data from (Marques et al., 2016) has been used for analysis. Read count data and meta data were downloaded from the USCS Cell Browser (https://mouse-oligo-het.cells.ucsc.edu). Counts were filtered and normalized using Scanpy (Wolf et al., 2018). Cells were identified as OPCs based on the "OPC" annotation in the meta data with high *Pdgfra* expression and no *Plp1* expression. Differential expression was identified by the *scanpy.tl.rank_genes_groups* command and genes with p value <.01 were subjected to DAVID online tool (Huang et al., 2009a, 2009b) to search for enriched GO terms. For Olig2^{neg} cells, only 7 genes ($p < .01$) were selected which were not adequate for GO analysis (Supplementary File S1).

4.13 | Statistical analysis

Data were analyzed with Graphpad Prism 9.0 and figures were generated with Adobe Indesign 2022. Animal numbers and the statistical parameters are indicated in the figure legends. Data were shown as mean ± SEM and the means of each group were compared. Briefly, for the comparisons between two groups but from the same mice (e.g., the contra- and ipsilateral sides, or Olig2^{pos} and Olig2^{neg} cells with BrdU or Ki67 expression), we performed two-tailed paired t-tests. For the comparisons among more than two groups, we employed one-way ANOVA analysis. For two-group comparison between different mice, two-tailed unpaired t-tests were performed.

AUTHOR CONTRIBUTIONS

Li-Pao Fang and Xianshu Bai conceived and designed the experiments; Xianshu Bai and Li-Pao Fang performed surgeries and kainate injections; Erika Meyer performed MCAO experiments; Li-Pao Fang, Qing Liu and Wenhui Huang performed Erasmus Ladder experiments. Li-Pao Fang and Qing Liu carried out slice preparations, immunohistochemistry, confocal imaging, and data analysis. Anja Scheller performed AxioScan imaging. Anna Welle performed analysis of single cell RNA transcriptomic data. Xianshu Bai and Frank Kirchhoff supervised the project; Xianshu Bai wrote the manuscript with input from the other authors.

ACKNOWLEDGMENTS

The authors are grateful to Daniel Schauenburg and Frank Rhode for their excellent animal husbandry and technical assistance. We thank Prof. Dr. Mengsheng Qiu (Institute of Life Sciences, Hangzhou Normal University, Hangzhou, China) for providing feedback on the manuscript. We are grateful to Dr. Hongkui Zeng (Allen Institute for Brain Science, Seattle, Washington, USA) for providing Rosa26-tdTomato reporter mice, Dr. Amit Agarwal (Institute for Anatomy and Cell Biology, Heidelberg University, Heidelberg, Germany) for providing Rosa26-GCaMP3 mice and Prof. Dr. Jacqueline Trotter (Molecular Cell Biology, Johannes-Gutenberg University, Mainz, Germany) for providing AN2/NG2 antibodies. Qing Liu was supported by a PhD student stipend from the Chinese Scholarship Council. Open Access funding enabled and organized by Projekt DEAL.

FUNDING INFORMATION

This work was supported by grants from the DFG (SPP 1757 to Frank Kirchhoff and SPP1757 Young Investigator grant to Xianshu Bai; FOR 2289 to Frank Kirchhoff and Anja Scheller, Project 462650276 to Wenhui Huang), the Romanian UEFISCDI (PCE 227; PN-III-P4-ID-PCE-2020-2477 to Frank Kirchhoff) and the University of Saarland (NanoBioMed Young Investigator Grant to Xianshu Bai, HOMFORexzellent2018 program to Xianshu Bai).

CONFLICT OF INTEREST

The authors declare no competing or financial interests.

DATA AVAILABILITY STATEMENT

The raw data are available from the corresponding authors upon reasonable request. Data of single cell RNA sequencing was submitted with the manuscript in Supplementary file.

ORCID

Li-Pao Fang https://orcid.org/0000-0002-7973-9523
Qing Liu https://orcid.org/0000-0002-5245-1474
Erika Meyer https://orcid.org/0000-0002-8425-6358
Anna Welle https://orcid.org/0000-0001-9915-2845
Wenhui Huang https://orcid.org/0000-0001-9865-0375
Anja Scheller https://orcid.org/0000-0001-8955-2634
Frank Kirchhoff https://orcid.org/0000-0002-2324-2761
Xianshu Bai https://orcid.org/0000-0002-4758-1645

REFERENCES

Bai, X., Zhao, N., Huang, W., Caudal, L., Zhao, R., Hirrlinger, J., Walz, W., Kirchhoff, F., & Scheller, A. (2021). After traumatic brain injury oligodendrocytes regain a plastic phenotype and can become astrocytes. *bioRxiv*, 2021.2006.2018.448919. https://doi.org/10.1101/2021.06.18.448919

Bedner, P., Dupper, A., Hüttmann, K., Müller, J., Herde, M.K., Dublin, P., Deshpande, T., Schramm, J., Häussler, U., Haas, C.A., Henneberger, C., Theis, M., & Steinhäuser, C. (2015). Astrocyte uncoupling as a cause of human temporal lobe epilepsy. *Brain*, *138*(Pt 5), 1208–1222. https://doi.org/10.1093/brain/awv067

Bergles, D. E., Roberts, J. D., Somogyi, P., & Jahr, C. E. (2000). Glutamatergic synapses on oligodendrocyte precursor cells in the hippocampus. *Nature*, *405*(6783), 187–191. https://doi.org/10.1038/35012083

Buffo, A., Vosko, M. R., Ertürk, D., Hamann, G. F., Jucker, M., Rowitch, D., & Götz, M. (2005). Expression pattern of the transcription factor Olig2 in response to brain injuries: Implications for neuronal repair. *Proceedings of the National Academy of Sciences of the United States of America*, *102*(50), 18183–18188. https://doi.org/10.1073/pnas.0506535102

Burman, D. D. (2019). Hippocampal connectivity with sensorimotor cortex during volitional finger movements: Laterality and relationship to motor learning. *PLoS One*, *14*(9), e0222064. https://doi.org/10.1371/journal.pone.0222064

Cai, J., Chen, Y., Cai, W. H., Hurlock, E. C., Wu, H., Kernie, S. G., Parada, L. F. & Lu, Q. R. (2007). A crucial role for Olig2 in white matter astrocyte development. *Development*, *134*(10), 1887–1899. https://doi.org/10.1242/dev.02847

Chen, Y., Miles, D. K., Hoang, T., Shi, J., Hurlock, E., Kernie, S. G., & Lu, Q. R. (2008). The basic helix-loop-helix transcription factor olig2 is critical for reactive astrocyte proliferation after cortical injury. *The Journal of Neuroscience*, *28*(43), 10983–10989. https://doi.org/10.1523/JNEUROSCI.3545-08.2008

Coats, S. R., Olashaw, N. E., & Pledger, W. J. (1994). Characterization of platelet-derived growth factor alpha receptor synthesis and metabolic turnover. *Cell Growth & Differentiation*, *5*(9), 937–942.

Dimou, L., Simon, C., Kirchhoff, F., Takebayashi, H., & Goetz, M. (2008). Progeny of Olig2-expressing progenitors in the gray and white matter of the adult mouse cerebral cortex. *Journal of Neuroscience*, *28*(41), 10434–10442. https://doi.org/10.1523/jneurosci.2831-08.2008

Fang, L. P., Zhao, N., Caudal, L. C., Chang, H. F., Zhao, R., Lin, C. H., Hainz, N., Meier, C., Bettler, B., Huang, W., Scheller, A., Kirchhoff, F., & Bai, X. (2022). Impaired bidirectional communication between interneurons and oligodendrocyte precursor cells affects social cognitive behavior. *Nature Communications*, *13*(1), 1394. https://doi.org/10.1038/s41467-022-29020-1

Galván, A. (2010). Neural plasticity of development and learning. *Human Brain Mapping*, *31*(6), 879–890. https://doi.org/10.1002/hbm.21029

Gautier, H. O., Evans, K. A., Volbracht, K., James, R., Sitnikov, S., Lundgaard, I., James, F., Lao-Peregrin, C., Reynolds, R., Franklin, R.J.M., & Káradóttir, R. T. (2015). Neuronal activity regulates remyelination via glutamate signalling to oligodendrocyte progenitors. *Nature Communications*, *6*, 8518. https://doi.org/10.1038/ncomms9518

Higashi, T., Tanaka, S., Iida, T., & Okabe, S. (2018). Synapse elimination triggered by BMP4 exocytosis and presynaptic BMP receptor activation. *Cell Reports*, *22*(4), 919–929. https://doi.org/10.1016/j.celrep.2017.12.101

Huang, D. W., Sherman, B. T., & Lempicki, R. A. (2009a). Bioinformatics enrichment tools: Paths toward the comprehensive functional analysis of large gene lists. *Nucleic Acids Research*, *37*(1), 1–13. https://doi.org/10.1093/nar/gkn923

Huang, D. W., Sherman, B. T., & Lempicki, R. A. (2009b). Systematic and integrative analysis of large gene lists using DAVID bioinformatics resources. *Nature Protocols*, *4*(1), 44–57. https://doi.org/10.1038/nprot.2008.211

Huang, W., Bai, X., Meyer, E., & Scheller, A. (2020). Acute brain injuries trigger microglia as an additional source of the proteoglycan NG2. *Acta Neuropathologica Communications*, *8*(1), 146. https://doi.org/10.1186/s40478-020-01016-2

Huang, W., Zhao, N., Bai, X., Karram, K., Trotter, J., Goebbels, S., Scheller, A., & Kirchhoff, F. (2014). Novel NG2-CreERT2 knock-in mice demonstrate heterogeneous differentiation potential of NG2 glia during development. *Glia*, *62*(6), 896–913. https://doi.org/10.1002/glia.22648

Jacobacci, F., Armony, J. L., Yeffal, A., Lerner, G., Amaro, E., Jovicich, J., Doyon, J., & Della-Maggiore, V. (2020). Rapid hippocampal plasticity supports motor sequence learning. *Proceedings of the National Academy of Sciences of the United States of America*, *117*(38), 23898–23903. https://doi.org/10.1073/pnas.2009576117

Jahn, H. M., Kasakow, C. V., Helfer, A., Michely, J., Verkhratsky, A., Maurer, H. H., Scheller, A., & Kirchhoff, F. (2018). Refined protocols of tamoxifen injection for inducible DNA recombination in mouse astroglia. *Scientific Reports*, *8*(1), 5913. https://doi.org/10.1038/s41598-018-24085-9

Kessaris, N., Fogarty, M., Iannarelli, P., Grist, M., Wegner, M., & Richardson, W. D. (2006). Competing waves of oligodendrocytes in the forebrain and postnatal elimination of an embryonic lineage. *Nature Neuroscience*, *9*(2), 173–179. https://doi.org/10.1038/nn1620

Kishida, N., Maki, T., Takagi, Y., Yasuda, K., Kinoshita, H., Ayaki, T., Noro, T., Kinoshita, Y., Ono, Y., Kataoka, H., Yoshida, K., Lo, E.H., Arai, K., Miyamoto, S., & Takahashi, R. (2019). Role of perivascular oligodendrocyte precursor cells in angiogenesis after brain ischemia. *Journal of the American Heart Association*, *8*(9), e011824. https://doi.org/10.1161/JAHA.118.011824

Komitova, M., Serwanski, D. R., Lu, Q. R., & Nishiyama, A. (2011). NG2 cells are not a major source of reactive astrocytes after neocortical stab wound injury. *Glia*, *59*(5), 800–809. https://doi.org/10.1002/glia.21152

Kupp, R., Shtayer, L., Tien, A. C., Szeto, E., Sanai, N., Rowitch, D. H., & Mehta, S. (2016). Lineage-restricted OLIG2-RTK signaling governs the molecular subtype of glioma stem-like cells. *Cell Reports*, *16*(11), 2838–2845. https://doi.org/10.1016/j.celrep.2016.08.040

Ligon, K. L., Kesari, S., Kitada, M., Sun, T., Arnett, H. A., Alberta, J. A., Anderson, D.J., Stiles, C.D., & Rowitch, D. H. (2006). Development of NG2 neural progenitor cells requires Olig gene function. *Proceedings of the National Academy of Sciences of the United States of America*, *103*(20), 7853–7858. https://doi.org/10.1073/pnas.0511001103

Lin, S. C., & Bergles, D. E. (2004). Synaptic signaling between GABAergic interneurons and oligodendrocyte precursor cells in the hippocampus. *Nature Neuroscience*, *7*(1), 24–32. https://doi.org/10.1038/nn1162

Liu, Q., Guo, Q., Fang, L. P., Yao, H., Scheller, A., Kirchhoff, F., & Huang, W. (2022). Specific detection and deletion of the sigma-1 receptor widely expressed in neurons and glial cells in vivo. *J Neurochem*. https://doi.org/10.1111/jnc.15693

Liu, Z., Hu, X., Cai, J., Liu, B., Peng, X., Wegner, M., & Qiu, M. (2007). Induction of oligodendrocyte differentiation by Olig2 and Sox10: Evidence for reciprocal interactions and dosage-dependent mechanisms. *Developmental Biology*, *302*(2), 683–693. https://doi.org/10.1016/j.ydbio.2006.10.007

Lu, F., Chen, Y., Zhao, C., Wang, H., He, D., Xu, L., Wang, J., He, X., Deng, Y., Lu, E.E., Liu, X., Verma, R., Bu, H., Drissi, R., Fouladi, M., Stemmer-Rachamimov, A.O., Burns, D., Xin, M., Rubin, J.B., & Lu, Q. R. (2016). Olig2-dependent reciprocal shift in PDGF and EGF receptor signaling regulates tumor phenotype and mitotic growth in malignant glioma. *Cancer Cell*, *29*(5), 669–683. https://doi.org/10.1016/j.ccell.2016.03.027

Lu, Q. R., Sun, T., Zhu, Z., Ma, N., Garcia, M., Stiles, C. D., & Rowitch, D. H. (2002). Common developmental requirement for Olig function indicates a motor neuron/oligodendrocyte connection. *Cell*, *109*(1), 75–86. https://doi.org/10.1016/s0092-8674(02)00678-5

Lu, Q. R., Yuk, D., Alberta, J. A., Zhu, Z., Pawlitzky, I., Chan, J., McMahon, A.P., Stiles, C.D., & Rowitch, D. H. (2000). Sonic hedgehog-regulated oligodendrocyte lineage genes encoding bHLH proteins in the mammalian central nervous system. *Neuron*, *25*(2), 317–329.

Madisen, L., Zwingman, T. A., Sunkin, S. M., Oh, S. W., Zariwala, H. A., Gu, H., Ng, L.L., Palmiter, R.D., Hawrylycz, M.J., Jones, A.R., Lein, E.S., & Zeng, H. (2010). A robust and high-throughput Cre reporting and characterization system for the whole mouse brain. *Nature Neuroscience*, *13*(1), 133–140. https://doi.org/10.1038/nn.2467

Maire, C. L., Wegener, A., Kerninon, C., & Nait Oumesmar, B. (2010). Gain-of-function of Olig transcription factors enhances oligodendrogenesis and myelination. *Stem Cells*, *28*(9), 1611–1622. https://doi.org/10.1002/stem.480

Marisca, R., Hoche, T., Agirre, E., Hoodless, L. J., Barkey, W., Auer, F., Castelo-Branco, G., & Czopka, T. (2020). Functionally distinct subgroups of oligodendrocyte precursor cells integrate neural activity and execute myelin formation. *Nature Neuroscience*, *23*(3), 363–374. https://doi.org/10.1038/s41593-019-0581-2

Marques, S., van Bruggen, D., Vanichkina, D. P., Floriddia, E. M., Munguba, H., Väremo, L., Giacomello, S., Falcão, A.M., Meijer, M., Björklund, Å.K., Hjerling-Leffler, J., Taft, R.J., & Castelo-Branco, G. (2018). Transcriptional convergence of oligodendrocyte lineage progenitors during development. *Developmental Cell*, *46*(4), 504–517. e507. https://doi.org/10.1016/j.devcel.2018.07.005

Marques, S., Zeisel, A., Codeluppi, S., van Bruggen, D., Mendanha Falcão, A., Xiao, L., Li, H., Häring, M., Hochgerner, H., Romanov, R.A., Gyllborg, D., Muñoz Manchado, A., La Manno, G., Lönnerberg, P., Floriddia, E.M., Rezayee, F., Ernfors, P., Arenas, E., Hjerling-Leffler, J., & Castelo-Branco, G. (2016). Oligodendrocyte heterogeneity in the mouse juvenile and adult central nervous system. *Science*, *352*(6291), 1326–1329. https://doi.org/10.1126/science.aaf6463

Mei, F., Wang, H., Liu, S., Niu, J., Wang, L., He, Y., Etxeberria, A., Chan, J.R., & Xiao, L. (2013). Stage-specific deletion of Olig2 conveys opposing functions on differentiation and maturation of oligodendrocytes. *The Journal of Neuroscience*, *33*(19), 8454–8462. https://doi.org/10.1523/JNEUROSCI.2453-12.2013

Nishiyama, A., Lin, X. H., Giese, N., Heldin, C. H., & Stallcup, W. B. (1996). Co-localization of NG2 proteoglycan and PDGF alpha-receptor on O2A progenitor cells in the developing rat brain. *Journal of Neuroscience Research*, *43*(3), 299–314. https://doi.org/10.1002/(SICI)1097-4547(19960201)43:3<299::AID-JNR5>3.0.CO;2-E

Orduz, D., Maldonado, P. P., Balia, M., Vélez-Fort, M., de Sars, V., Yanagawa, Y., Emiliani, V., & Angulo, M. C. (2015). Interneurons and oligodendrocyte progenitors form a structured synaptic network in the developing neocortex. *eLife*, *4*, 1-20. https://doi.org/10.7554/eLife.06953

Patel, C., Meadowcroft, M. D., Zagon, I. S., & McLaughlin, P. J. (2020). [Met5]-enkephalin preserves diffusion metrics in EAE mice. *Brain Research Bulletin*, *165*, 246–252. https://doi.org/10.1016/j.brainresbull.2020.10.015

Paukert, M., Agarwal, A., Cha, J., Doze, V. A., Kang, J. U., & Bergles, D. E. (2014). Norepinephrine controls astroglial responsiveness to local circuit activity. *Neuron*, *82*(6), 1263–1270. https://doi.org/10.1016/j.neuron.2014.04.038

Pfeiffer, S. E., Warrington, A. E., & Bansal, R. (1993). The oligodendrocyte and its many cellular processes. *Trends in Cell Biology*, *3*(6), 191–197. https://doi.org/10.1016/0962-8924(93)90213-k

Rowitch, D. H., & Kriegstein, A. R. (2010). Developmental genetics of vertebrate glial-cell specification. *Nature*, *468*(7321), 214–222. https://doi.org/10.1038/nature09611

Saab, A. S., Neumeyer, A., Jahn, H. M., Cupido, A., Šimek, A. A., Boele, H. J., Scheller, A., Le Meur, K., Götz, M., Monyer, H., Sprengel, R., Rubio, M.E., Deitmer, J.W., De Zeeuw, C.I., & Kirchhoff, F. (2012). Bergmann glial AMPA receptors are required for fine motor

coordination. *Science*, *337*(6095), 749–753. https://doi.org/10.1126/science.1221140

Scheller, A., Bai, X., & Kirchhoff, F. (2017). The role of the oligodendrocyte lineage in acute brain trauma. *Neurochemical Research*, *42*(9), 2479–2489. https://doi.org/10.1007/s11064-017-2343-4

Segel, M., Neumann, B., Hill, M. F. E., Weber, I. P., Viscomi, C., Zhao, C., Young, A., Agley, C.C., Thompson, A.J., Gonzalez, G.A., Sharma, A., Holmqvist, S., Rowitch, D.H., Franze, K., Franklin, R.J.M., & Chalut, K. J. (2019). Niche stiffness underlies the ageing of central nervous system progenitor cells. *Nature*, *573*(7772), 130–134. https://doi.org/10.1038/s41586-019-1484-9

Serrano-Regal, M. P., Luengas-Escuza, I., Bayón-Cordero, L., Ibarra-Aizpurua, N., Alberdi, E., Pérez-Samartín, A., Matute, C., & Sánchez-Gómez, M. V. (2020). Oligodendrocyte differentiation and myelination is potentiated via GABA. *Neuroscience*, *439*, 163–180. https://doi.org/10.1016/j.neuroscience.2019.07.014

Spitzer, S. O., Sitnikov, S., Kamen, Y., Evans, K. A., Kronenberg-Versteeg, D., Dietmann, S., de Faria, O. Jr., Agathou, S., & Káradóttir, R. T. (2019). Oligodendrocyte progenitor cells become regionally diverse and heterogeneous with age. *Neuron*, *101*(3), 459–471.e455. https://doi.org/10.1016/j.neuron.2018.12.020

Su, Y. S., Veeravagu, A., & Gerald, G. (2016). Neuroplasticity after traumatic brain injury. In D. Laskowitz & G. Grant (Eds.), *Translational research in traumatic brain injury*. CRC Press/Taylor and Francis Group.

Takebayashi, H., Nabeshima, Y., Yoshida, S., Chisaka, O., & Ikenaka, K. (2002). The basic helix-loop-helix factor olig2 is essential for the development of motoneuron and oligodendrocyte lineages. *Current Biology*, *12*(13), 1157–1163.

Tatsumi, K., Takebayashi, H., Manabe, T., Tanaka, K. F., Makinodan, M., Yamauchi, T., Makinodan, E., Matsuyoshi, H., Okuda, H., Ikenaka, K., & Wanaka, A. (2008). Genetic fate mapping of Olig2 progenitors in the injured adult cerebral cortex reveals preferential differentiation into astrocytes. *Journal of Neuroscience Research*, *86*(16), 3494–3502. https://doi.org/10.1002/jnr.21862

Trotter, J., Karram, K., & Nishiyama, A. (2010). NG2 cells: Properties, progeny and origin. *Brain Research Reviews*, *63*(1–2), 72–82. https://doi.org/10.1016/j.brainresrev.2009.12.006

Van Der Giessen, R. S., Koekkoek, S. K., van Dorp, S., De Gruijl, J. R., Cupido, A., Khosrovani, S., Dortland, B., Wellershaus, K., Degen, J., Deuchars, J., Fuchs, E.C., Monyer, H., Willecke, K., De Jeu, M.T., & De Zeeuw, C. I. (2008). Role of olivary electrical coupling in cerebellar motor learning. *Neuron*, *58*(4), 599–612. S0896-6273(08)00262-6 [pii] 10.1016/j.neuron.2008.03.016.

Viganò, F., & Dimou, L. (2015). The heterogeneous nature of NG2-glia. *Brain Research*, *1638*, 129–137. https://doi.org/10.1016/j.brainres.2015.09.012

Viganò, F., Möbius, W., Götz, M., & Dimou, L. (2013). Transplantation reveals regional differences in oligodendrocyte differentiation in the adult brain. *Nature Neuroscience*, *16*(10), 1370–1372. https://doi.org/10.1038/nn.3503

Wang, H., Xu, L., Lai, C., Hou, K., Chen, J., Guo, Y., Sambangi, A., Swaminathan, S., Xie, C., Wu, Z., &Sambangi, A., Swaminathan, S., Xie, C., Wu, Z., & Chen, G. (2021). Region-specific distribution of Olig2-expressing astrocytes in adult mouse brain and spinal cord. *Molecular Brain*, *14*(1), 36. https://doi.org/10.1186/s13041-021-00747-0

Wegener, A., Deboux, C., Bachelin, C., Frah, M., Kerninon, C., Seilhean, D., Wieder, M., Wegner, M., & Nait-Oumesmar, B. (2015). Gain of Olig2 function in oligodendrocyte progenitors promotes remyelination. *Brain*, *138*(Pt 1), 120–135. https://doi.org/10.1093/brain/awu375

Wimmer, I., Scharler, C., Zrzavy, T., Kadowaki, T., Mödlagl, V., Rojc, K., Tröscher, A.R., Kitic, M., Ueda, S., Bradl, M., & Lassmann, H. (2019). Microglia pre-activation and neurodegeneration precipitate neuroinflammation without exacerbating tissue injury in experimental autoimmune encephalomyelitis. *Acta Neuropathologica Communications*, *7*(1), 14. https://doi.org/10.1186/s40478-019-0667-9

Wolf, F. A., Angerer, P., & Theis, F. J. (2018). SCANPY: large-scale single-cell gene expression data analysis. *Genome Biology*, *19*(1), 15. https://doi.org/10.1186/s13059-017-1382-0

Xiao, Y., Petrucco, L., Hoodless, L. J., Portugues, R., & Czopka, T. (2022). Oligodendrocyte precursor cells sculpt the visual system by regulating axonal remodeling. *Nature Neuroscience*, *25*, 280–284. https://doi.org/10.1038/s41593-022-01023-7

Zhang, K., Chen, S., Yang, Q., Guo, S., Chen, Q., Liu, Z., Li, L., Jiang, M., Li, H., Hu, J., Pan, X., Deng, W., Xiao, N., Wang, B., Wang, Z.X., Zhang, L., & Mo, W. (2022). The oligodendrocyte transcription factor 2 OLIG2 regulates transcriptional repression during myelinogenesis in rodents. *Nature Communications*, *13*(1), 1423. https://doi.org/10.1038/s41467-022-29068-z

Zhang, X., Liu, Y., Hong, X., Li, X., Meshul, C. K., Moore, C., Yang, Y., Han, Y., Li, W.G., Qi, X., Lou, H., Duan, S., Xu, T.L., & Tong, X. (2021). NG2 glia-derived GABA release tunes inhibitory synapses and contributes to stress-induced anxiety. *Nature Communications*, *12*(1), 5740. https://doi.org/10.1038/s41467-021-25956-y

Zhou, Q., & Anderson, D. J. (2002). The bHLH transcription factors OLIG2 and OLIG1 couple neuronal and glial subtype specification. *Cell*, *109*(1), 61–73. https://doi.org/10.1016/s0092-8674(02)00677-3

Zhou, Q., Wang, S., & Anderson, D. J. (2000). Identification of a novel family of oligodendrocyte lineage-specific basic helix-loop-helix transcription factors. *Neuron*, *25*(2), 331–343.

Zhu, X., Zuo, H., Maher, B. J., Serwanski, D. R., LoTurco, J. J., Lu, Q. R., & Nishiyama, A. (2012). Olig2-dependent developmental fate switch of NG2 cells. *Development*, *139*(13), 2299–2307. https://doi.org/10.1242/dev.078873

SUPPORTING INFORMATION

Additional supporting information can be found online in the Supporting Information section at the end of this article.

How to cite this article: Fang, L.-P., Liu, Q., Meyer, E., Welle, A., Huang, W., Scheller, A., Kirchhoff, F., & Bai, X. (2023). A subset of OPCs do not express Olig2 during development which can be increased in the adult by brain injuries and complex motor learning. *Glia*, *71*(2), 415–430. https://doi.org/10.1002/glia.24284